Nano Today 27 (2019) 178–197

Contents lists available at ScienceDirect

Nano Today

journal homepage: www.elsevier.com/locate/nanotoday

Metal-organic frameworks as emerging platform for supporting isolated single-site catalysts

Wenshi Zhao, Guodong Li*, Zhiyong Tang*

CAS Key Laboratory of Nanosystem and Hierarchical Fabrication, CAS Center for Excellence in Nanoscience, National Center for Nanoscience and Technology, Beijing, 100190, PR China

ARTICLE INFO

Article history:
Received 1 March 2019
Received in revised form 8 April 2019
Accepted 21 May 2019
Available online 5 June 2019

Keywords:
Single-site catalyst
Metal-organic frameworks
Isolated
Synergistic catalysis
Nanopore
Confinement effect

ABSTRACT

Isolated heterogeneous single-site catalysts have been attracted great interest in diverse catalytic reactions because of their uniform and distinct geometric and electronic structure. Among various porous supports, metal-organic frameworks (MOFs), with molecular level structure control and modularity, offer the versatile platforms for supporting isolated single-site catalysts. Owing to the well-defined anchoring sites lying in the nodes, ligands or nanopores of MOFs, the single-site catalysts could be grafted precisely without protection by bulky ligands. More interestingly, together with the nanopore confinement effect of MOFs, single-site catalysts could exhibit the excellent performances in terms of catalytic activity, selectivity and stability. In this review, we focus on summarizing the recent advances in the precise design, synthesis, characterization and catalytic applications of isolated single-site catalysts supported by MOFs and elucidating the relationship between structure and performance of single-site catalysts. Finally, we give a perspective on controllable synthesis of isolated single-site catalysts supported by MOFs as well as their catalytic applications.

Contents

* Corresponding authors.
E-mail addresses: liguodong@nanoctr.cn (G. Li), zytang@nanoctr.cn (Z. Tang).

https://doi.org/10.1016/j.nantod.2019.05.007
1748-0132/

Introduction

Isolated heterogeneous single-site catalysts have been intensively investigated in diverse reactions via thermo-, electro- and photo-driven modes, because they possess the distinct advantages in the maximum atom utilization, unsaturated coordination environments, unique electronic structures and metal-support interactions over conventional metal nanoparticles [1–5]. Furthermore, they have great potential to integrate the distinct advantages of homogeneous and heterogeneous catalysts into a single counterpart. Generally, the simplest and most common method of producing heterogeneous single-site catalysts is to anchor catalytically active atoms, ions or molecular complexes onto the surfaces of solid supports, such as silica, metal oxides and carbon materials [6–9]. However, the anchoring sites are often limited and disordered, thus leading to non-uniform distribution of single-site catalysts throughout the solid supports. This also tends to be complicated by intermolecular interactions between catalytic sites and surface functionalities. Therefore, it is challengeable to prevent intermolecular deactivation in the development of single-site catalysts, since homogeneous metal catalysts generally need to be stabilized with bulky, elaborately designed ligands. Such steric protection is important for stabilizing weak-field ligand-coordinated metal catalysts, particularly for late first-row transition metals in the weak-field coordination environment consisting of oxygen-donor atoms [10]. However, steric protecting groups often block the contact of substrates with active sites, thus impeding the catalytic performance [11,12]. To address above, an alternative route for obtaining high-performance single-site metal catalysts is to immobilize the catalytic species in structurally regular porous solid supports characteristic of catalytic site isolation without relying on bulky ligands [13,14]. Obviously, it is highly desirable to develop novel porous materials possessing well-ordered and precisely controlled nanostructures for supporting single-site catalysts.

Among various porous materials such as silica, metal oxides and carbon materials, metal-organic frameworks (MOFs), also known as porous coordination polymers (PCPs), which are synthesized by self-assembly of metal ions or clusters with ditopic or polytopic organic linkers, have aroused great interest in heterogeneous catalysis, due to their intriguing features of extraordinarily large surface area, tunable pore dimensions, well-defined metal nodes, adjustable chemical composition and surface functionality [15–20]. The unlimited possible combinations of metal-oxo clusters and organic linkers allow access to reticular structures with tunable pore sizes and functional properties [21–25]. Furthermore, the precision commonly achieved in the chemical modification and the ability to expand the metrics without changing the underlying topology have not been achieved by conventional porous supports such as carbon, zeolites and metal oxides [26–28]. Obviously, MOFs represent the excellent scaffolds for incorporating single-site catalysts. The catalytic sites can be placed in the well-defined positions of MOFs through either rational design of metal nodes, organic linkers and environments of pores or post-synthetic modification such as solvothermal deposition in MOFs (SIM) and atomic layer deposition in MOFs (AIM) [29–32]. By using pre-metalated organic struts or via post-synthetic metalation of bridging linkers, MOFs have provided a highly tunable platform to engineer single-site solid catalysts for many organic transformations that cannot be performed by traditional porous inorganic materials [6,33,34]. Furthermore, the secondary building units (SBUs) of MOFs consisting of inorganic oxide clusters can be used as oxygen-donor ligands, thus providing an unprecedented opportunity for developing robust, site-isolated, metal catalysts in a weak field coordination environment [35,36]. Also, the tunable nanopores in MOFs could endow the single-site catalysts with size-selective catalytic performances in the confined space. For examples, UiO-66 is characteristic of the free diameter of tetrahedral cage of 0.8 nm and octahedral cage of 1.1 nm, and the cages are connected by triangular windows with a diameter of 0.6 nm [37]. The aperture size of UiO-67 is 0.8 nm with an octahedral cavity of 1.1 nm^3 in solvent accessible volume, where the largest dimension (vertex to vertex of the octahedron) is close to 1.88 nm [38]. There are three kinds of nanopores in NU-1000, in which the triangular and hexagonal nanopores of 1.2 and 3.1 nm, respectively, are aligned along the a-axis, while rhomboid nanopores of 1.0 nm are aligned along the c-axis [39]. Also, MIL-101(Cr) owns free internal diameters of 2.9 and 3.4 nm and corresponding microporous windows of 1.2 and 1.6 nm, respectively [40].

The synthetic tunability of MOFs makes it possible to fine-tune electronic and steric properties of catalytic active sites, whereas the structure regularity and site homogeneity of MOFs greatly facilitate mechanistic studies of catalytic reactions [41,42]. The well-defined single-site catalysts are regarded as ideal model catalysts to identify active sites and understand reaction process at a molecular level [43]. Altogether, the highly ordered arrangements of the metal nodes and organic linkers as well as the well-defined nanopore structures of MOFs make them as ideal substrates to support atomically dispersed metal sites located in the metal nodes, linkers and nanopores.

With the rapid development of modern characterization techniques, single-site catalysts supported by MOFs can be identified accurately. Moreover, combined with variable structure design and synthesis, we can move forward steps to exploring the relationships of structure and performance and realize “catalysts formation by design” [13]. In this review, we focus on the recent progress of MOFs as emerging platform to support active single sites for catalysis. First, the precise design and synthesis of MOFs for supporting single-site catalysts are described via various methods (Fig. 1). Second, different techniques for characterizing single-site catalysts are discussed. Third, we review the catalytic applications of isolated single-site catalysts in various reactions and discuss the relationships between structure and performance combined with accurate characterization. Finally, we give a perspective on isolated single-site catalysts supported by MOFs as well as their catalytic applications in the future.

Synthesis of MOFs supported isolated single-site catalysts

Single-site catalysts supported by metal nodes in MOFs

Generally, metal nodes built by metal oxide clusters of atomic precision usually act as Lewis acid sites, such as $ZrO_{6\text{-}8}$ [43,44], $Zr_6O_4(\mu_3\text{-}OH)_4$ [45,46], and $Zr_8O_8(\mu_2\text{-}OH)_4$ nodes [36,47], which creates an electron-deficient environment for single-site catalysts, and moreover, the uniform distribution of anchoring sites makes it as an ideal substrate for atom layer disposition of active sites [48]. More importantly, isolated single-site metal catalysts supported by metal nodes are free from intermolecular deactivation without protection by bulky, elaborately designed ligands, which

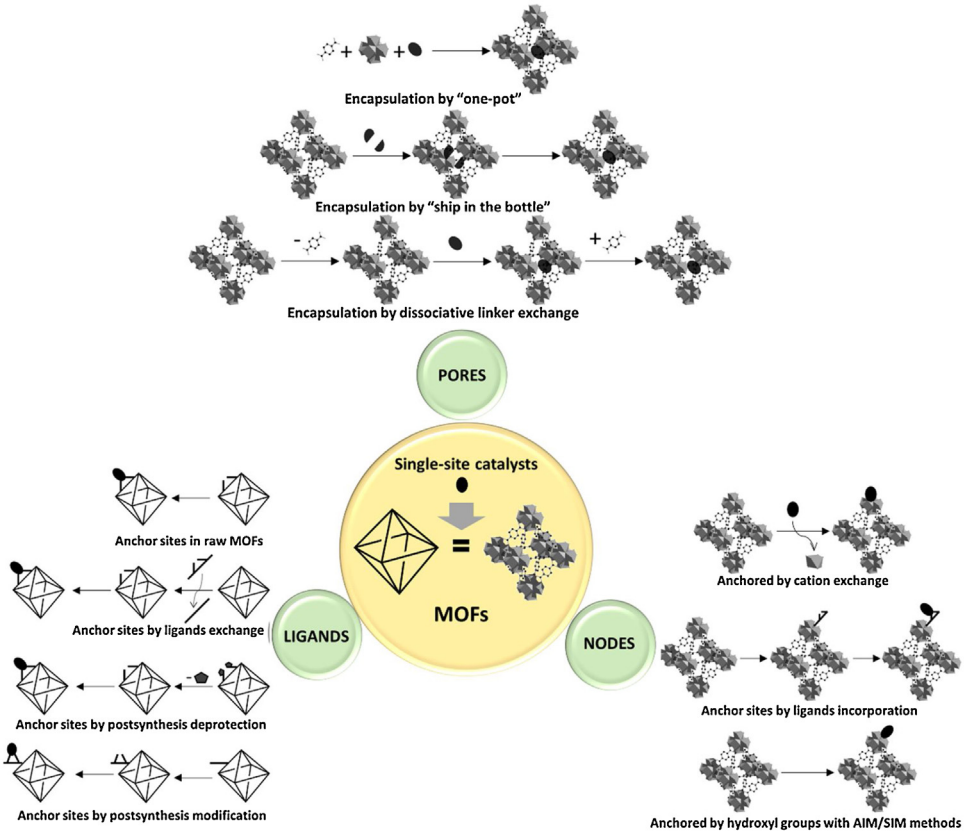

Fig. 1. Scheme of different methods for supporting single-site catalysts on the ligands, nodes and in the pores of MOFs.

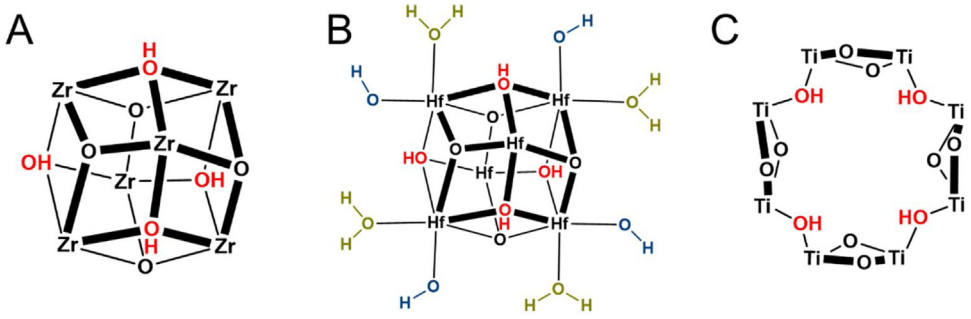

Fig. 2. Reactive hydrogen sites with different activity (like water, terminal hydroxyl groups and bridged hydroxyl groups) on the SUB of (A) UiO-66, (B) NU-1000 and (C) MOF-125.

cannot be achieved by conventional porous supports. To date, there are three possible strategies to graft single-site catalysts onto the metal nodes of MOFs. First, the coordinatively unsaturated metal nodes can act as binding sites to anchor additional ligands for supporting single-site catalysts [49]. Second, the hydroxyl groups and H_2O, which are molecularly coordinated on the metal nodes of some MOFs (Fig. 2), can provide the anchoring points for metal ions or organometallic complexes [6]. Third, single-site catalysts can be introduced into the metal nodes by substitution with the metal ions under weak coordination between metal nodes and ligands [50]. Altogether, the isolated anchoring sites provided by the metal nodes of MOFs offer great potential to produce structurally characterizable catalysts.

Solvent-assisted ligand incorporation on metal nodes

Metal nodes are commonly associated with transition metals that likely introduce Lewis acidity, and they can be exposed and further modified with additional ligands to support isolated single-site catalysts [51]. For examples, Hupp *et al.* reported missing-linker sites on the metal nodes of NU-1000, which is composed of SBUs, $Zr_6(\mu_3\text{-}O)_4(\mu_3\text{-}OH)_4(OH)_4(H_2O)_4$, and 1,3,6,8-tetrakis(p-benzoicacid)pyrene (H_4TBAPy) [48,52], could anchor 2,2′-bipyridine ligands by reaction with the HCl salt of 5-methylphosphonate-2,2′-bipyridine ligands, followed by deprotonation of 2,2′-bipyridine ligands with NEt_3 and then chelated with $NiCl_2$, denoted as NU-1000-bpy-$NiCl_2$ [53]. Inductively coupled plasma atomic emission spectroscopy (ICP-OES) analysis indicates a stoichiometry of ~1.5 [Ni] per Zr_6 node, suggesting a near-complete formation of supported (bpy)$NiCl_2$ species. This linker incorporation methodology took advantage of the ability of the $Zr_6(\mu_3\text{-}O)_4(\mu_3\text{-}OH)_4(OH)_4$ nodes of NU-1000 to be readily modified through reactions between the free Zr-OH moieties (or missing-linker sites) on the node and incoming carboxylic or phosphonic acid-containing ligands. Also, MIL-101 synthesized by trivalent metal ions coordinating with 1,4-dicarboxybenzene (BDC) is an ideal support because of its abundant open metal sites upon

activation and high stability [54]. The chromium nodes of MIL-101 can be post-synthetically modified with amine and pyridyl species to support catalytically active sites. Nguyen et al. reported that MIL-101 acts as the scaffold for post-synthesis incorporation of catechols that can be metallated [55]. Dopamine is a normal catechol-bearing grafting agent since it possesses a nucleophilic amino group that can coordinate to unsaturated chromium(III) centers, denoted as dop-MIL-101. Dop-MIL-101 was then reacted with vanadylacetylacetonate ($VO(acac)_2$) to afford a dark-brown vanadium-modified framework (V(dop)-MIL-101) that retained crystallinity. ICP-OES showed a V/Cr ratio of only 0.13 ± 0.02. Like metal catalysts, Lewis Pairs (LPs) can be anchored on the coordinatively unsaturated metal nodes of MOFs as single-site catalysts as well. The LP, which is composed of $B(C_6F_5)_3$ and 1,4-diazabicyclo[2.2.2]octane (DABCO), is grafted onto metal nodes by strong coordination interaction between the LP and open Cr^{3+} sites. After reaction, the electron density of Cr^{3+} increases, suggesting the successful incorporation of LP. The SEM and EDS elemental mapping analyses in different scales demonstrate the even distribution of LP in MOFs without the presence of accumulation in the particular regions [56].

Hydroxyl groups on metal nodes as anchoring sites

MOFs with free hydroxyl groups have aroused wide attention due to their potential to anchor catalysts in an analogous manner to traditional metal-oxo supports. Active hydroxyl groups and H_2O molecules on the nodes of MOFs like DUT-5, MIL-125, MOF-808, NU-1000 and UiO [45,46,48,57–60], could act as versatile binding sites for single-site catalysts like metal ions and organometallic complexes. Among these protonolytic sites, the bridged hydroxyl groups are less active due to weak acidity. For example, Farha et al. reported that a highly electrophilic single-site d^0 Zr-benzyl catalytic center, tetrabenzyl zirconium ($ZrBn_4$), was isolated on the nodes of Hf-NU-1000 (with the formula, $[Hf_6(\mu_3\text{-}O)_4(\mu_3\text{-}OH)_4(OH)_4(H_2O)_4]$) by reactions with acid -OH and $-OH_2$ sites. The well-defined nanopores and nanostructure of Hf-NU-1000-ZrBn remained after modification and single Zr sites are distributed evenly about 2.4 Zr sites per Hf_6 node on average. However, the μ_3-OH didn't attend the modification process due to less acidity [61]. On the same hydroxyl groups of the nodes in NU-1000, single molybdenum(VI) oxide sites are formed from $Mo(am)_2(im)_2$ in solutions under inert atmosphere [62]. ICP-OES measurements showed the metal loading of 2.8 ± 0.3 Mo per Zr_6 node. Recently, Behm et al. reported a facile way to support $CuCl_2$ on the node of UiO-66, in which one linker per one Zr_6 cluster was missing and the resulting defect sites were terminated by acetate and —OH/—OH_2 groups with a molecular formula as $Zr_6O_4(OH)_4(BDC)_5(CH_3COO)_{0.7}(H_2O)_{1.3}(OH)_{1.3}$ [63]. The Cu ion could be anchored on the terminal hydroxyl groups after heating UiO-66 in a DMF solution of $CuCl_2{\cdot}2H_2O$ at 85 °C overnight. Independent of the excess of $CuCl_2{\cdot}2H_2O$ used in the synthesis, the incorporation of Cu in Cu/UiO-66 with a Cu : Zr_6 atomic ratio of 0.8 remained same due to the limited hydroxyl groups. Farha *et al.* showed that single-atom-based vanadium catalysts were introduced on the node of Hf-MOF-808 (with the formula $[Hf_6(\mu_3\text{-}O)_4(\mu_3\text{-}OH)_4(OH)_6(H_2O)_6]$) and Zr-NU-1000 using solvothermal deposition method, which features only one vanadium per node [13]. The nodes of UiO-66 with the formula $[Zr_6(\mu_3\text{-}O)_4(\mu_3\text{-}OH)_4]$ can also support single vanadium site with hydroxyl group generated from defects caused by linker missing instead of inert μ_3-OH [64]. ICP-AES indicated a V loading of $\tilde{0}.1 \pm 0.01$ V/Zr [64]. Gates et al. reported that $Ir(C_2H_4)_2(C_5H_7O_2)$ complexes reacted with -OH on nodes generated by defects in UiO-66/67 to give site-isolated $Ir(C_2H_4)_2$ complexes, each anchored to the node by two Ir-O node bonds [65]. Farha et al. synthesized Hf-MOF-808-V and Zr-NU-1000-V by mixing pre-existing Hf-MOF-808 and Zr-NU-1000 with vanadyl acetylacetonate ($V(O)(acac)_2$) in a methanol solution. The structures of vanadium species were found to be quite different in Hf-MOF-808-V versus Zr-NU-1000-V [13]. In Hf-MOF-808-V, three types of crystallographically nonequivalent single-atom vanadium sites were observed, binding to the Hf_6-node in chelating mode (V1, V2, and V3). The crystallographically estimated loadings were 0.48(V1), 0.54(V2), and 0.48(V3) vanadium per Hf_6-node, aligning well with the loadings determined by ICP-OES. For Zr-NU-1000-V, multiple single-atom vanadium species were observed on the bridging position (V1) and the monodentate positions (V2, V3) of the Zr_6 node. The estimated loadings were 0.56(V1), 0.40(V2), and 0.12(V3) vanadium per Zr_6 node, a single atom per node, but each occupying one of three possible sites. Heterometallic active sites could also be deposited onto the nodes of MOFs simultaneously by this method. For examples, Lu et al. reported that heterobimetallic cobalt-aluminum single sites were installed on the nodes of NU-1000 fully and evenly (one Al and Co per node) from the precursors (py_3tren)-AlCoMe in solutions via an acid-base reaction with the hydroxyl groups. After removing py_3tren under 300 °C, the coordinatively unsaturated heterobimetallic oxide core were generated [66]. With the similar methods, post-synthetic grafting of RhGa(py_3tren) onto NU-1000 was achieved by soaking the MOF in a benzene solution of (py_3tren)GaRhX (X = Me or OPh; py_3tren = $[N(CH_2CH_2N\text{-}(o\text{-}C_5H_4N))_3]^{3-}$) to afford RhGa($py_3$tren)-NU-1000. ICP-AES analyses revealed Rh and Ga loadings of 3.3 and 2 wt%, respectively, and a Zr : Rh : Ga mole ratio of 6 : 1.07 : 1.01 [67]. As for the less acidic μ-OH groups, they can react with organometallics with higher activity to anchor single-site catalysts. For example, Lin et al. reported $MgMe_2$ could react with μ-OH groups and the single-site μ_4-OMgMe was formed on the nodes of UiO-69-NO_2 [10]. ICP-MS analysis of the digested MOF-MgMe revealed 100% metalation at the $Zr_3(\mu_3\text{-}OH)$ sites, corresponding to four Mg centers per Zr_6 node (Fig. 3A). Crystallinity of UiO-69-NO_2 was maintained upon metalation as evidenced by the PXRD patterns.

In addition to directly reacting with free hydroxyl groups on the metal nodes, another way is to deprotonate hydroxyl group with organic lithium regents, and then the less acidic bridged hydroxyl groups on nodes can anchor various single non-noble metal ions (Fig. 3B). For examples, Lin et al. reported that after deprotonation with nBuLi followed by reaction with $CoCl_2$ or $FeBr_2$ in THF, the $Zr_3(\mu_3\text{-}OH)$sites in SBUs of UiO-68, $Zr_6(\mu_3\text{-}O)_4(\mu_3\text{-}OH)_4$, afforded the single Co (or Fe) sites supported by UiOs [6]. Fitting the extended X-ray absorption fine structure (EXAFS) regions of UiO-CoCl and UiO-FeBr demonstrated that the Co and Fe centers were coordinated to three SBU oxygen atoms and one halogen atom. ICP-MS analysis revealed 100% metalation at $Zr_3(\mu_3\text{-}OH)$ sites, corresponding to four Co/Fe per Zr_6 node. Further activated by $NaEt_3BH$, the active single catalytic sites, $Zr_3\text{-}\mu_3\text{-}CoH$, are formed. The same group reported that Zr_{12}-TPDC MOF of the formula $Zr_{12}O_8(\mu_3\text{-}OH)_8(\mu_2\text{-}OH)_6(TPDC)_9$ forms through dimerizing two Zr_6 clusters via six μ_2-OH groups as a result of the reduction of H_2TPDC concentration by addition of water. Zr_{12}-TPDC MOF was treated with $LiCH_2SiMe_3$ to deprotonate both the μ_2-OH and μ_3-OH sites in Zr_{12}-SBU, then reacted with a $CoCl_2$ solution in THF to afford Zr_{12}-TPDC-CoCl as a deep-blue solid. Crystallinity of the MOF was maintained after metalation, as indicated by the similarity between the PXRD patterns of Zr_{12}-TPDC and Zr_{12}-TPDC-CoCl. ICP-MS analysis revealed the presence of 11.2 ± 0.6 Co per Zr_{12} cluster, corresponding to complete metalation of all eight μ_3-OLi sites to form eight (Zr_3O^-)CoCl, and all six μ_2-OLi sites to form three $[(Zr_2O^-)_2(Zr_3O)CoCl]Li$, to give the complete formula of $Zr_{12}(\mu_3\text{-}O)_5[(\mu_3\text{-}O^-)CoCl]_8[(\mu_2\text{-}O^-)_2(\mu_3\text{-}O)CoCl]_3Li_3(TPDC)_9$ [29]. With the similar method, other SBU of Zr-MOFs, like $Zr_8(\mu_2\text{-}O)_8(\mu_2\text{-}OH)_4$, can also be modified with the single Co and Fe sites, and moreover, the different structure of nodes endows the single-site catalysts with the distinct activities [36].

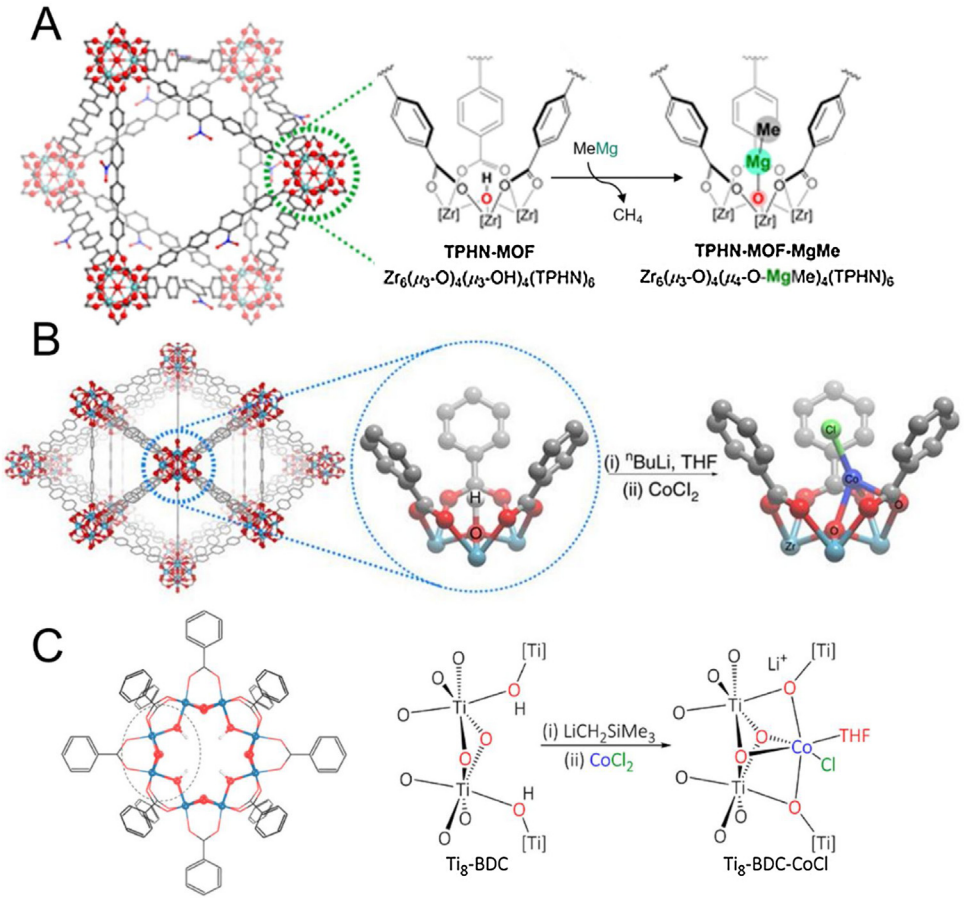

Fig. 3. Scheme of the postsynthetic metalation of the SBUs of (A) TPHN-MOF with Me_2Mg. Reprinted with permission from Ref. [10] Copyright (2016) American Chemical Society. (B) UiO-68 with $CoCl_2$. Reprinted with permission from Ref. [6] Copyright 2016, Springer Nature. (C) MIL-125(Ti) with $CoCl_2$. Reprinted with permission from Ref. [41] Copyright (2018) American Chemical Society.

The nodes of MIL-125, $Ti_8(\mu_2\text{-}O)_8(\mu_2\text{-}OH)_4$, can support single-site Co catalyst [41,68]. After partially reduced by $LiCH_2SiMe_3$, $Ti^{III}{}_2Ti^{IV}{}_6$-BDC-CoH is formed, in which electron-rich high-spin Co^{2+} centers are stabilized by electron-donating Ti^{3+}-oxo ligands. Ti_8-BDC was first deprotonated with $LiCH_2SiMe_3$ to generate a $Ti_8O_8(OLi)_4(BDC)_6$ intermediate and then metalated with $CoCl_2$ to generate Ti_8-BDC-CoCl as a turquoise solid (Fig. 3C). ICP-MS demonstrates that the Co content in the metalated MOF was determined to be 0.7 Co per Ti_8 node [41].

Cation exchange at the SBUs

Cation exchange at the SBUs is an alternative way for introducing single-site metal catalysts into a well-defined coordination environment even when analogous molecular coordination compounds are elusive or MOFs with those metals of interest are unavailable by direct synthesis. Generally, this method is suitable for the SBUs with a weak field ligand environment [50]. For examples, Dincă et al. reported the first example of a ferric hyponitrite in Fe-exchanged Zn_4O(terephthalate)$_3$ (MOF-5) [69]. Later, they prepared a series of materials known as (Cl)M-MOF-5 that arise from Ti^{3+}, V^{3+}, V^{2+}, Cr^{3+}, Cr^{2+}, Mn^{2+}, Fe^{2+}, or Ni^{2+} replacing a four-coordinate Zn^{2+} cation in each cluster of MOF-5 ($Zn_4O(BDC)_3$) (Fig. 4A). The same group reported that a single Mn^{2+} site was supported by distorted all-oxygen ligand field after partial substitution of Zn^{2+} in MOF-5 and the high-spin Mn^{IV}-oxo species formed after the oxidation of Mn^{2+} sites by $^tBuSO_2PhIO$. The active high-spin Mn^{IV}-oxo species are stabilized by the relatively weak ligand fields provided by the SBU [35]. ICP-MS analysis of Mn^{II}-MOF-5 samples gave a ratio of Mn to Zn about 1 : 15, corresponding to one Mn^{II} ion in every four SBUs and a formula unit of $Mn_{0.25}Zn_{3.75}(BDC)_3$ ($Mn^{II}{}_{high}$-MOF-5). Cohen et al. reported that the tetrahedral Zn^{2+} sites in ZIF-8 (Zn-(MeIm)) and ZIF-71 (Zn-(Cl_2Im)) could be replaced by Mn^{2+} ions [70]. In addition, the SBU of MFU-4*l* ($ZnZn_4Cl_4(BTDD_6)$) can undergo cation exchange to support various single metal sites [71]. It is noted that the SBU of MFU-4*l* consists of five zinc atoms: one central atom coordinated octahedrally by six nitrogen atoms, and four peripheral tetrahedral zinc atoms coordinated by three triazole groups and one chloride that points toward the center of the pore (Fig. 4B). The single V^{2+} sites can be isolated in the SBU by exchange with unsaturated peripheral Zn^{2+}, and moreover, the Ti, Cr, Mn, Cu, Fe, Co and Ni ions can also be introduced via this method. Further, side-ligands on the exchanged ions could be exchanged upon thermal treatment with structure intact such as nitrene intermediate involved from Co^{2+}-azide units in the SBU and Cu^+ formation from Cu^{2+}-fluoride units [72–74]. The isomorphous partial substitution of Zn^{2+} ions in the SBU of MFU-4*l* leads to frameworks with the general formula $[M_xZn_{5-x}Cl_4(BTDD)_3]$, in which x = 2, M = Mn, Fe, Co or Ni, BTDD = bis(1,2,3-triazolato-[4,5-b], [4′,5′-i])dibenzo-[1,4]-dioxin. Subsequent exchange of chloride ligands by nitrite, nitrate, triflate, azide, isocyanate, formate, acetate, or fluoride leads to a variety of MFU-4*l* derivatives [73]. The materials exchanged with VCl_4, and with $VCl_3(THF)_3$ showed nearly identical edge energies and pre-edge features, both of which are consistent with a vanadium (IV) oxidation state and are denoted as V^{IV}-MFU-4*l*. By contrast, the material exchanged with $VCl_2(py)_4$ exhibits an edge energy most consistent with vanadium (II), which is labeled as V^{II}-MFU-4*l*. The resulting materials showed good structural retention

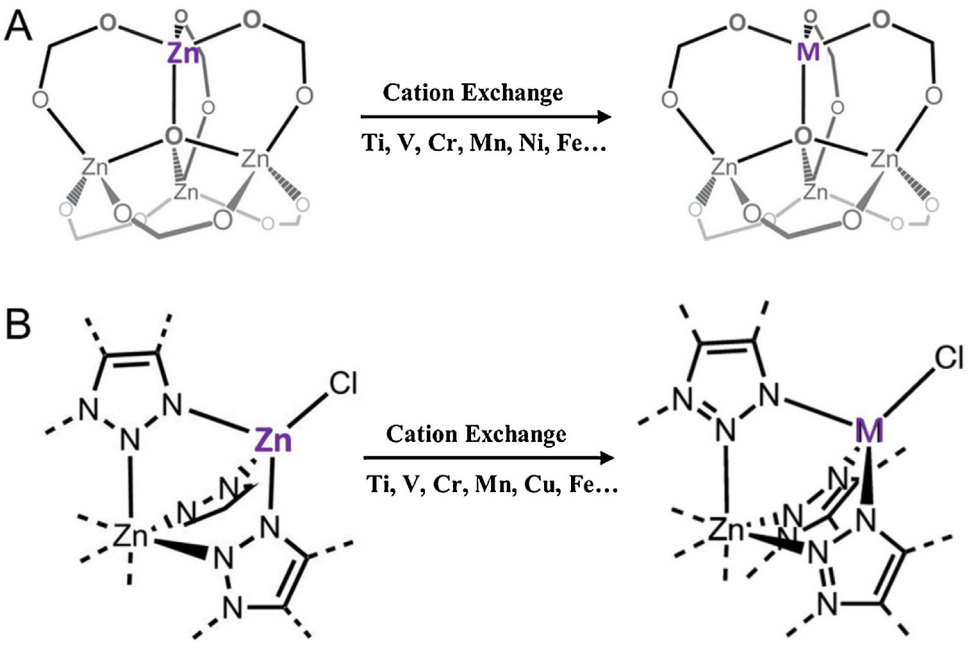

Fig. 4. Single-site catalysts anchoring on the nodes in (A) MOF-5 and (B) MFU-4*l* obtained via cation exchange with other metal ions. Reprinted with permission from Ref. [72] Copyright (2016) American Chemical Society.

by powder X-ray diffraction and gas sorption analysis [75]. The site-selective postsynthetic exchange occurred in MOFs with different SBUs. Moorthy et al. prepared a semi-rigid MOF with 2,4,6-Tris(4-(α-carboxy)methoxyphenyl)mesitylene and $Zn(NO_3)_2{\cdot}6H_2O$ in a mixture solution of DEF, EtOH and H_2O. Two kinds of SBU existing in this MOF, the infinite one is composed of Zn^{2+} ions bridged by μ-O and carboxylate groups and the other one is an isolated Zn^{2+} coordinated to four carboxylate groups in a monodentate fashion. Site-selective post-synthetic exchange of discrete Zn^{2+} occurs in the solution of Fe^{3+}, Ru^{3+}, Cu^{2+} or Co^{2+} solutions in a single crystal-to-single crystal (SCSC) fashion, but Zn^{2+} ions in the other kind of SUB is unable to realize this process [76]. It is noted that all the metal nodes partially substituted by active metal sites could preserve the basic coordination scaffold as a result of the geometric constraints imposed by the MOF crystal lattice.

Atomic layer deposition (ALD) in MOFs

In addition to SIM methods, atomic layer deposition (ALD) is a vapor-phase synthetic technique for constructing the single-site catalysts. The key conceptual advance that ALD embodies over chemical vapor deposition/infiltration is that precursor molecules deposit only at chemically reactive surface sites (Fig. 5A and 5B), and these reactions are self-limiting [48,52,59,77,78]. For examples, Martinson et al. reported that Pt species were deposited on the nodes of NU-1000 via AIM method with spatial and dimensional homogeneity. Unlike growth of Pt on porous supports such as HZSM-5 and MIL-101 with trimethyl(methylcyclopentadieny)platinum(IV) ($MeCpPtMe_3$), self-limiting behavior inhibits the formation of nanoparticles. The component of Pt species generated in MOFs is determined by synthesis temperature. The main component is Pt clusters at 160 °C and single Pt atoms arise at a lower temperature of 115 °C [79]. Isolated by organic linkers, the single Pt sites exhibit high operando stability and resistance to sintering up to 200 °C. The samples prepared at 115 °C and 160 °C result in average loadings of 0.15 and 2.5 Pt per Zr_6 node, respectively, with uniform distribution of Pt (relative to Zr and O) throughout NU-1000 crystals, while preserving structural integrity [79]. The steric and electronic properties of single metal sites isolated on the nodes of NU-1000 can be tuned with auxiliary ligands or additional metals to modify catalytic properties. For examples, Hupp et al. grafted election-withdrawing ligands of hexafluoroacetylacetonate ($Facac^-$) and acetylacetonate ($Acac^-$) on the nodes of NU-1000 by displacing node aquand hydroxo ligands and each ligand chelates a single Zr ion according to single crystal diffraction (Fig. 5C). With retention of hydroxyl groups, Ni sites could be anchored via AIM method [80]. The AIM method can also be applied for tuning the properties of nodes in NU-1000 by modification with aluminum. New binding sites, terminal OH groups bridging Al and Zr atoms, arose after modification, which could support single-site Ir catalysts [81]. Farha et al. explored the differences in modifying the nodes of NU-1000 with single Nb(V) oxide sites by ALD (AIM) and solution-phase grafting in a MOF (SIM). After metalation, the surface area decreased obviously for both methods. The pore size was observed no change by AIM method, but the mesopore size was reduced by SIM, demonstrating that different synthesis methods lead to different local structures. Further with Difference Envelope Density (DED), the Nb^{5+} atoms were unfirmly distributed in the lateral cavities between the two adjacent Zr_6 nodes via AIM, while Nb oxide dimers were formed in cavities by SIM method [82]. The nanopore geometry of the NU-1000 support has a greater influence on the distribution of transition metal species deposited through AIM than the initial distribution of the available $-OH_x$ reaction sites. Deposition occurs preferentially at sites within the pores of NU-1000, where adsorption of the ALD reagent molecules is most favorable. For Zn-ALD in NU-1000, deposition occurs at only half of the original $-OH_x$ sites with selective ALD in the smallest pores of the NU-1000 framework, but not in the intermediate triangular or large hexagonal channels [83].

Altogether, after activation and removing coordinated solvent molecules, the metal nodes can generate open metal sites for additional ligands to provide various binding sites for single-site catalysts [84]. The terminal hydroxyl groups and H_2O molecules coordinated on the node can fix single metal sites under inert environment by reactions with active organometallic precursors along with release little organic molecules and heterobimetallic deposition can also be realized by this method. As for the less acidic bridged hydroxyl groups, few complexes can be isolated directly

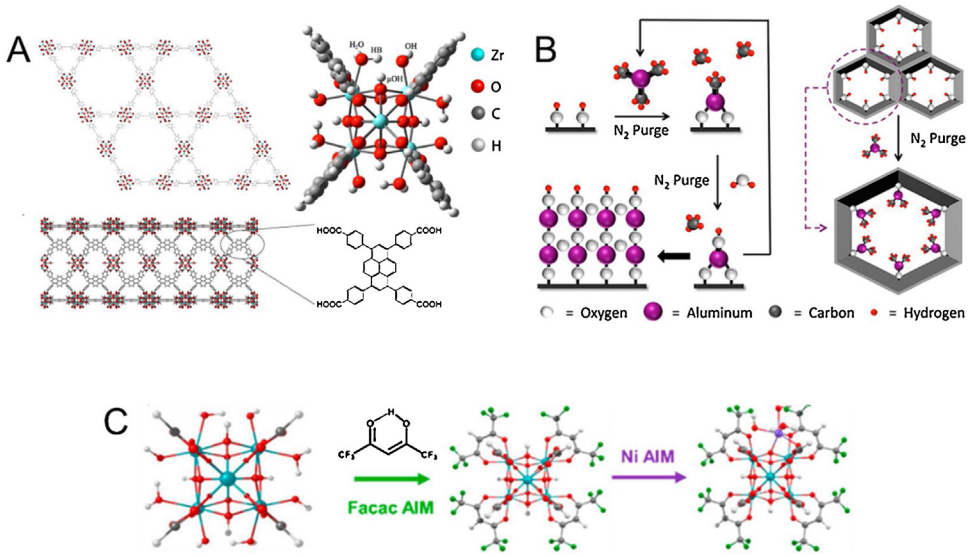

Fig. 5. (A) Zr_6-based framework NU-1000. Reprinted with permission from Ref. [52] Copyright (2015) American Chemical Society. (B) Thin Film ALD deposition on a surface and metalation by ALD in a MOF (AIM). Reprinted with permission from Ref [48]. Copyright (2013) American Chemical Society. (C) Schematic depiction of installation of the monoanionic $Facac^-$ ligand and Ni ions to the Zr_6 nodes of NU-1000. Reprinted with permission from Ref. [80] Copyright (2018) American Chemical Society.

except some very active precursors like $MgMe_2$. While after deprotonation of bridged hydroxyl groups with organic lithium regents, the transition metal ions can be anchored on the nodes. With a weak field ligand environment or containing coordinatively unsaturated metal sites, the transition metals on the SBU can be substituted to support single-site catalysts and mixed metal nodes are formed. Various metal ions (Ti, Cr, Mn, Cu, Fe, Co and Ni ions) can be introduced in the SUB with the structure preservation in a single crystal-to-single crystal (SCSC) fashion. The incorporation of metal ions with higher coordination number can generate active unsaturated metal sites, of which the catalytic activity is influenced by the synergy effect of mixed metal nodes and side-ligands. However, this method is mainly limited to the transition metal ions and few noble metal ions can be incorporated in the SBU. All these methods are applied in solutions, in which removing adsorbed solvent molecules is hindered. So, the AIM (ALD in MOFs) shows great potential in atomically precise deposition of precursor molecules at the nodes of NU-1000 with self-limiting reactions. Various metals like Pt, Ni, Al, Nb are supported on the nodes successfully and their activity can be tuned by auxiliary ligands or additional metals deposited. But due to the stringent criteria of ALD, only NU-1000 is applied in this method and many other suitable MOFs are needed to be explored.

Single-site catalysts supported by organic linkers in MOFs

The organic linkers in MOFs provide various binding sites, such as N, O, P and S (Fig. 6), for supporting isolated single-site catalysts. With delicate design and synthesis of ligands, many kinds of binding sites can be incorporated into MOFs [85]. However, some organic groups are very reactive or with large size, which prohibit the formation of target MOFs and others are too fragile to bear the intensive synthesis condition of MOFs. To address above, the post-syntheticdeprotection (PSD), solvent-assisted linker exchange (SALE) and post-synthesis modification (PSM) are developed [86–91]. However, after introduction of single-site catalysts, the pore volume is decreased significantly, which will limit the full modification of MOFs and mass transportation in reactions. The possible strategy is to adopt longer ligands or dope the ligands without binding sites in MOFs to avoid pore entrance blocking [92].

Pre-modifying linker with anchoring sites

The pyridine series ligands are widely used as chelating ligands with strong binding affinity to base metals, but they do not provide adequate steric protection around metal centers to afford efficient base-metal catalysts [93,94]. The orthogonal bpy-type ligands comprising the MOF structs are site-isolated and can stabilize base-metal complexes for catalysis. Typically, Zr-nodes based MOFs with pyridine moieties are good supports for single-site catalysts due to the excellent thermal and chemical stability. For examples, Matsuoka et al. reported that the single-site Cu^{2+} ions are anchored on the ligands of MOFs, 2,2′-bipyridine-5,5′-dicarboxylate, by stirring with UiO-67-bpy in acetonitrile solutions [95]. The loading amount was determined to be 3.3 wt% for Zr-MOF-bpy-$CuBr_2$, indicating that 20.6% of the bpy units were metallated with Cu in the Zr-MOF-bpy framework. As for metal complexes with large size, the open channels in UiO-67-bpy would shrink too largely to finish the full modification of MOFs and the mass transportation of substrates and products would be limited. To address above, Lin *et al.* adopted 4,4′-(2,2′-bipyridine-5,5′-diyl)dibenzoateas ligands to generate larger pores for meeting the steric demand of active (bpy)$Re(CO)_3Cl$ reaction centers and attenuate the impact of reduced pores [96]. Another way to prevent pore blockage upon metalation is doping the ligands with no binding sites like 4,4′-biphenyldicarboxylate in the synthesis process and the loading of active sites can be tuned [38,93,97]. Huang et al. synthesized Co-Ru-UiO-67(bpy) by mixing $ZrCl_4$, 2,2-bipyridine-5,5-dicarboxylic acid (H_2bpdcy), Rudcbpy ($[Ru(dcbpy)-(bpy)_2]Cl_2$), $CoCl_2$, and glacial acetic acid in DMF solution. The concentrations of Co and Ru in Co-Ru-UiO-67(bpy) are 5.68×10^{-7} and 1.08×10^{-7} mol/mg, respectively, corresponding to the elemental ratio of Co to Ru about 5.26 [98]. To mimic the phenanthroline (Phen) ligand environment in homogeneous iridium/Phen catalysts, a Phen-containing linker, 1,10-phenanthroline-3,8-dicarboxylic acid (PhenDC), can be used in place of BPDC to synthesize the microporous UiO-67 support. Farha et al. reported that UiO-67-Mix is metallated with [Ir(1,5-cyclooctadiene)μ-Cl)]$_2$) ([Ir(COD)(μ-Cl)]$_2$ to yield initially a green inactive catalyst UiO-67-Mix-Ir-green, which contains Ir(I) and is spontaneously oxidized in air to an orange pre-catalyst UiO-67-Mix-Ir. ICP-MS indicated that about two iridium atoms per Zr_6 node were incorporated into the UiO-67-Mix MOF. The oxidation state of iridium in UiO-67-Mix-Ir was confirmed by X-ray pho-

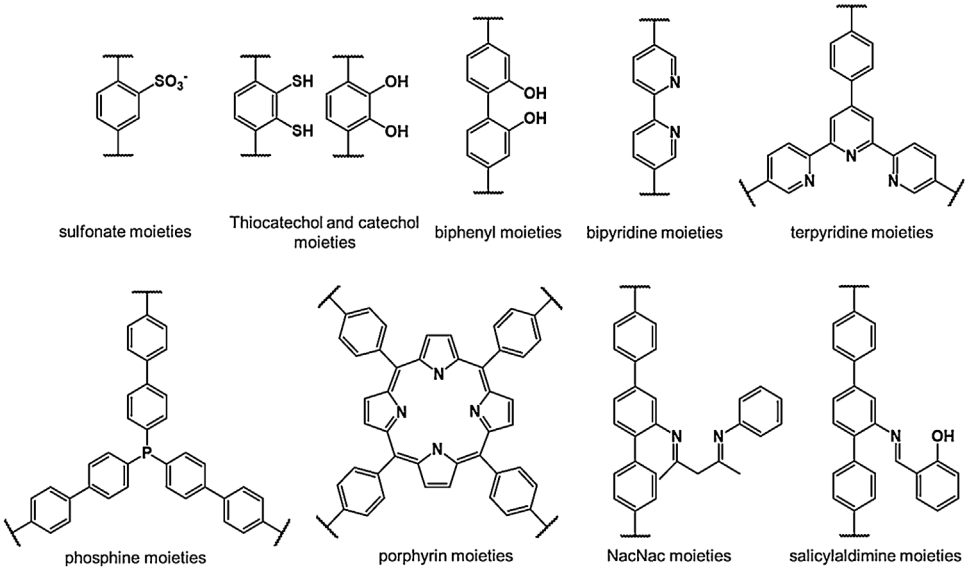

Fig. 6. Different kinds of binding sites on the ligands of MOFs.

toelectron spectroscopy and X-ray absorption spectroscopy as +3 [38].

Except for bipyridine, terpyridine moieties were also incorporated into MOFs. For example, Liu et al. employed 2-TriPP-COOH (4′-(4-carboxyphenyl)-2,2′:6′,2″-terpyridine) as ligands and holmium(III) as nodes to assemble Ho-MOFs. At the same time, the terpyridyl moieties, which don't coordinate with nodes in the skeleton of Ho-MOF, are available to anchor single metal ions [99]. Through post-synthetic modification of the palladium precursor $PdCl_2(CH_3CN)_2$ with Ho-MOF, a well-defined Pd-Ho-MOF was obtained. ICP-MS experiments indicated that more than 2.51 wt% of the palladium was anchored to Ho-MOF [99]. Lin et al. synthesized on kind of MOLs (Metal-Organic Layers, two-dimensional MOFs), whose thickness was only 1.2 ± 0.2 nm, with Hf^{4+} cluster, benzene-1,3,5-tribenzoate (BTB) and 4′-(4-benzoate)-(2,2′,2″-terpyridine)-5,5″-dicarboxylate (TPY) by taking advantage of the matching shape and size between TPY. The resultant TPY-MOL with 30% TPY (based on the total number of tridentate ligands) was metalated with $FeBr_2$ activated by $NaBHEt_3$. ICP-MS analysis indicated that the final Fe-TPY-MOL catalyst contains 100% of Fe with respect to TPY [100].

Porphyrin unit with N_4 structure possesses the well-defined square-planar anchoring sites for single-site catalysts. With four nitrogen atoms, porphyrin moieties are capable to fix metal ions tightly to stand harsh reaction conditions and they can act as anchoring sites for single-site catalysts [101,102]. For example, Wang et al. prepared the zirconium-porphyrinic MOF hollow nanotubes (HNTM) by a solvothermal reaction of zirconium chloride ($ZrCl_4$), tetrakis(4-carboxyphenyl)porphyrin (TCPP), benzoic acid, and trace H_2O in *N,N*-dimethylformamide (DMF) solvent at 120 °C, on which a series of single noble-metal (Ir, Pt, Ru, Au, Pd) ions could be immobilized, and moreover, different metal ions could be introduced into the structure at the same time [103]. The structure and crystallinity of HNTM are well maintained after single atoms were immobilized according to their similar PXRD patterns.

Phosphine-ligated transition metal complexes play an important role in the development of organometallic chemistry and homogeneous catalysis. The phosphine binding sites can be introduced into MOFs with delicate design and synthesis. For example, Lin et al. incorporated isolated phosphine sites in P_1-MOF composed of Zr-oxo SBUs and triarylphosphine-derived tricarboxylate linkers [104]. Further, the single (mono)phosphine-M (M = Rh and Ir) sites in MOFs are generated via post-synthetic metalation by taking advantage of the isolation of phosphine sites. Another kind of phosphine site is designed in PCM-101 composed of tris(p-carboxylato)triphenylphosphine and secondary pillaring groups coordinated to $[M_3(OH)]^{5+}$ nodes (M = Co, Ni), in which R_3P: sites were formed in trans-conformation. The transition metal ions (Cu^+ and Au^+) can be isolated by the R_3P: sites [105]. The exact structure of these composites elucidated by single crystal X-ray diffraction indicates that the liner P-AuCl complexes are generated and the parent framework would distort with high loading of AuCl, while $(CuBr)_2$ squares can insert in the P_2 pockets with retention of host structure.

Sulfonated MOFs can act as the anionic framework host for supporting the cationic components. Grigoropoulos et al. reported that Crabtree's catalyst $[Ir(cod)(PCy_3)(py)][PF_6]$ was anchored on the sulfonate groups in sulfonated MIL-101 by cation exchange with Na^+ ions [106]. After encapsulation, the content of Ir was about 2.28 wt%, and moreover, the MOF complexes' crystallinity and particle morphology were almost retained only with slight reduction of surface area and nanopore size.

Post-modifying linker with anchoring sites

With the long skeleton, the ligands can be modified with diverse moieties like salicylaldimine and then construct the MOFs [107]. However, the ligands turn more flexible after modification with the delicate moieties, which suppresses the formation of MOFs. The post-synthesis modification (PSM) of anchoring sites becomes necessary. Amino groups are very reactive in many reactions and many functional groups could be introduced into MOFs via the amino groups on the ligands. For example, Li et al. reported that the terpyridyl moieties (2,2′:6′,2″-terpyridine, tpy) were incorporated into the ligands of MIL-101-NH_2(Cr) by "click" post-functionalization as binding sites for single-site catalysts. The azido group derived from amino group was modified by employing the efficient azide-alkyne cycloaddition protocol (CuAAC) with 4′-ethynyl-2,2′:6′,2″-terpyridine and then the MIL-101(Cr)-tpy was generated [92]. And the maleic anhydride groups and β-diketiminate moieties can be fixed in MIL-53(Al) and UiO-69-NH_2 by reactions with amino groups, respectively [108,109]. Another reactive group is chloromethylene, which was functionalized with an effective single-site catalysts, $Co(dmgH)_2$(4-HEP)Cl complexes

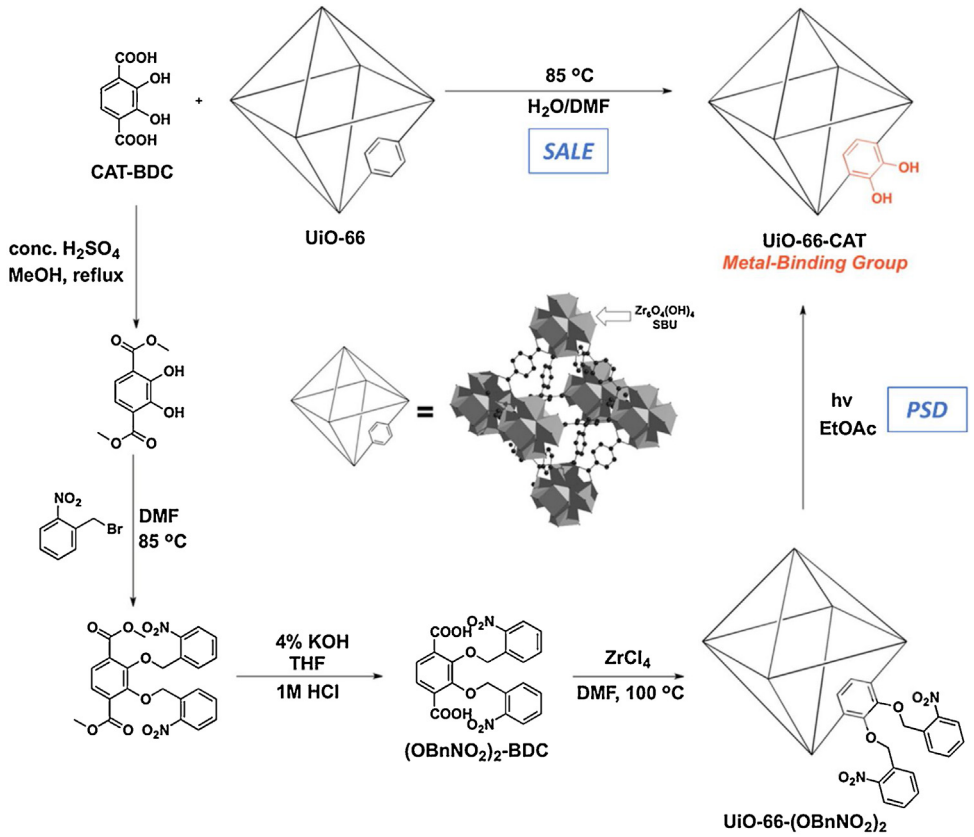

Fig. 7. Synthesis of UiO-66-CAT via PSD and PSE. Reprinted with permission from Ref. [112] Copyright (2014) American Chemical Society.

(dmgH = dimethylglyoxime. 4-HEP = 4-(2-hydroxyethyl)pyridine), in MIL-101(Cr) [110].

Some ligands with oxygen containing binding site can't be applied in the synthesis of MOFs directly, which would hinder the formation of target MOFs. To avoid the interference of these functional groups, the ligands with protection of these groups are applied. These anchoring sites would deprotect automatically or by the post-synthetic deprotection (PSD) method [85]. For example, biphenol linkers, which are protected by acetic, are incorporated into ANL1, a reticular MOF of UiO-67, synthesized by solvothermal reaction of bpdcOAc (2,2′-bis(acetoxy)-1,1′-biphenyl-4,4′-dicarboxylic acid) and H_2bpdc (1,1′-biphenyl-4,4′-dicarboxylic acid) ligands with $ZrCl_4$ in DMF and acetic acid. The acetate protecting groups could be removed automatically during the synthesis process to expose the biphenol binding sites and further fix single-site catalysts [111].

Catechol is one of the most widely used chelators in coordination chemistry and immobilization of catechol moieties in MOFs would provide ideal binding sites for highly unsaturated mono(catecholato) metal complexes [112]. Due to the two hydroxyl groups, the 2,3-dihydroxyterephthalic acid (CATBDC) can't be applied in the synthesis of UiO-66-CAT. Instead, the 2,3-Bis((2-nitrobenzyl)oxy)-1,4-benzene dicarboxylic acidis was applied in the synthesis and the photochemically driven PSD of 2-nitrobenzylprotection groups was used to generate free catechol groups. However, the protection of CATBDC need too many steps and the PSD method enabled only little part of catechol moieties into UiO-66 and provided the limited binding sites due to large protection groups [112]. Another way to incorporate the catechol moieties in the UiO is exchanging 1,4-benzene dicarboxylic acid (BDC) in the skeleton of UiO-66 with CATBDC via the solvent-assisted linker exchange (SALE) methods. SALE could be readily controlled to modulate the degree of catechol with simple operations (Fig. 7). Similarly, a soft thiocatechol motif, stable, but highly unsaturated metal sites could also be incorporated in UiO-66 via SALE method [113]. Immobilized thiocatechol ligands on the UiO-66-TCAT provide an excellent platform to achieve accessible and unsaturated mono(thiocatecholato) metal centers. The metalation of 40% thiocatechol-functionalized UiO-66-TCAT using $Pd(OAc)_2$ in CH_2Cl_2 afforded dark-brown solids. The crystallinity of UiO-66-PdTCAT was maintained upon metalation. ICP-OES confirmed an atomic ratio of 1 : 0.18 : 0.85 for Zr : Pd : S in the metal-loaded sample, confirming that 42% of thiocatechol sites was metalated. The ligands pre-chelated single-site catalysts can also be incorporated into MOFs by SALE method. For example, Fontecave et al. reported that parts of ligands in UiO-67, bpydc (2,2′-bipyridine-5,5′-dicarboxylic acid) were exchanged by $Cp^*Rh(bpydc)Cl_2$ [114]. Although SALE is more convenient, efficient, and controllable than the PSD, a lot of active sites are exposed on the surface, which may remove the confinement effect of nanopores in MOFs and weaken the selectivity in some reactions.

Altogether, the diverse organic ligands with easy tunability can provide various binding sites for single-site catalysts. The simplest way to incorporate homogeneous catalysts is to tune the coordination groups onto linkers of MOFs such as the porphyrin, phosphines ligands and bipyridine groups. The delicate binding sites can also be generated by post-synthetic modification (PSM) with reactive groups on ligands such as halogen, aldehyde and amino groups [115,116]. The linkers with no binding sites are necessary in the MOFs to facilitate mass transfer because of the decreased pore size by the incorporation of single-site catalysts. Some binding sites in ligands like hydroxyl groups are unable to be incorporated in MOFs directly, so the protection of groups is required, and the groups can be released by post-synthetic deprotection (PSD) method. But the process would be tedious with low loading of single-site catalysts when this method is applied for complicated functional groups

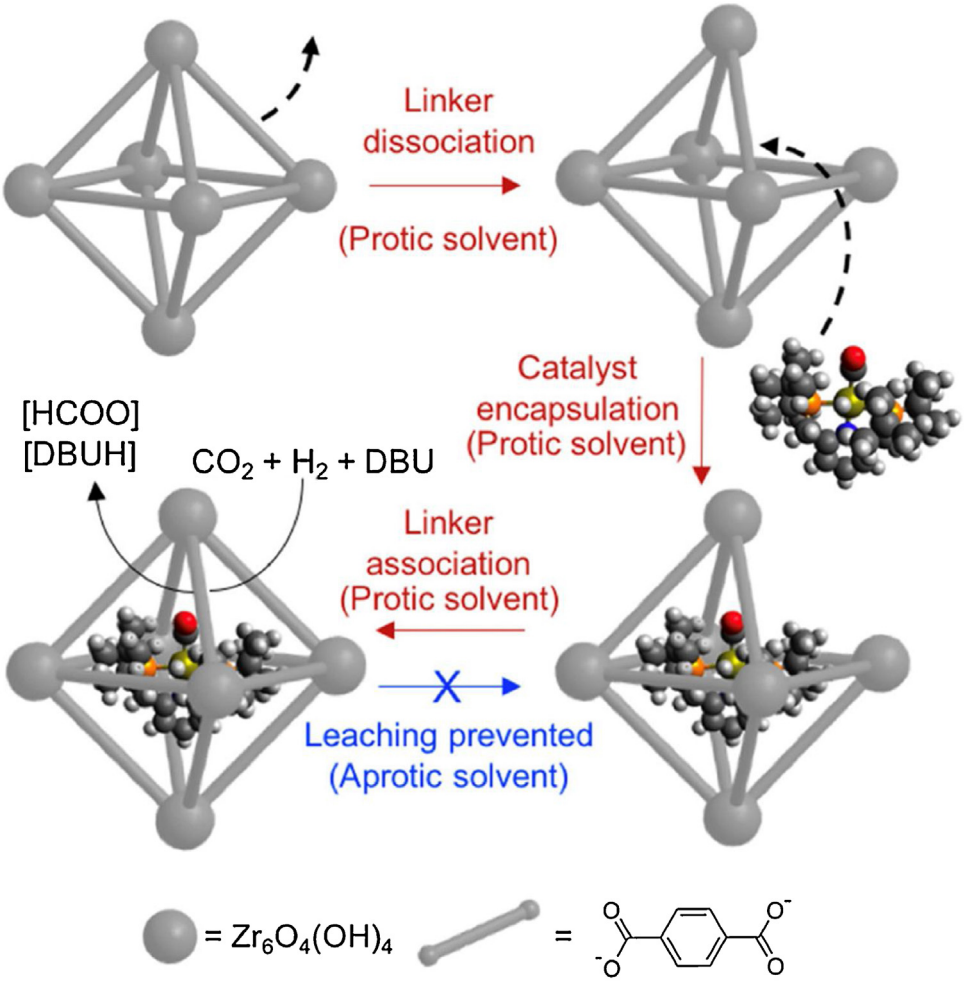

Fig. 8. Single-site catalysts located inside nanopores of MOFs via aperture-opening encapsulation. Reprinted with permission from Ref. [120] Copyright (2018) American Chemical Society.

such as catechol moieties. The solvent-assisted linker exchange (SALE) would facilitate the incorporation of ligands with binding site and then anchor the single-site catalysts with tunable loading. The ligands chelated with single-site catalysts can also exchange the ligands of prime MOFs directly. The SALE method is more convenient, efficient, and controllable than the PSD, but there are many single-site catalysts distributing in the surface of MOFs, which may lose selectivity compared with those confined inside nanopores.

Single-site catalysts located in nanopores of MOFs

As for single-site catalysts with large size, they can be encapsulated by the nanopores of MOFs. For examples, Notestein *et al.* reported that NU-1000 could encapsulate a high weight loading of phosphotungstic acid (PTA), while it remained intact [39]. The PTA is located in the small triangular channels and electrostatically bound to the node via one of the three H^+ of the PTA. The high loading of PTA pops opens the structure of catalysts, while composite with low loading of PTA collapses during preheating procedure because of strong interaction between PTA and Zr oxide clusters.

Larsen *et al.* reported a facile way to selectively fix Fe_4SP (Fe(3+) tetrakis(4-sulphonatophenyl)porphyrin) within specific cages of HKUST-1 by mixing the precursors of HKUST-1 and Fe_4SP during the synthesis process [117]. The metalloporphyrin was fixed in the octahedral cage, which fitted with the size and symmetry of HKUST-1, while the remaining cavities could allow small molecules to diffuse and contact the active site for catalysis like channels in heme proteins. The loading extent of porphyrin can be controlled, and the maximal loading could reach ~66% (cavity loading) at the saturating porphyrin concentration.

Confining single-site catalysts into the nanopores of MOFs can be implemented by postsynthetic methods. Das *et al.* reported a postsynthetic method to isolate one molecule of MnTD ($[(terpy)Mn(\mu\text{-}O)_2Mn](terpy)]^{3+}$; terpy: 2,2′:6′,2″-terpyridine), an efficient catalyst for water oxidation, in each nanopore of MIL-101 [118]. MnTD was successfully located in the nanopores of MIL-101 by first loading the cages with terpy over a period of 18 h, followed by addition of $Mn(OAc)_2$ and, in parallel, K-oxone in stoichiometric amounts. Finally, the content of MnTD was 10 wt% in the obtained product. According to the crystal structure, the size of MnTD with the counterions was $1.4 \times 1.2 \times 0.8\ nm^3$. It is noted that MIL-101 possessed maximum internal diameters of 2.9 nm and 2.4 nm and pore apertures with maximum free diameters of 1.2 nm and 1.5 nm, meaning that only one molecule was isolated in each pore and leaching was prohibited. Also, this was further verified by spectroscopic characterization [119].

Tsung et al. reported that the complexes (tBuPNP)Ru(CO)HCl (tBuPNP = 2,6-is((di-tert-butylphosphino)methyl)pyridine) larger than the aperture size of UiO-66 were introduced into the pores by taking advantage of aperture-opening events that occur as a result of dissociative linker exchange reactions (Fig. 8) [120]. The aperture-opening events were highly dependent on the identity of the solvent used. As for protic solvents like methanol, the linker dissociation and association occurred rapidly and the single-site

catalysts were encapsulated during the above two procedures. As contrast, aprotic solvent such as DMF was applied to suppress these processes and avoid leaking of catalysts during the reaction tests. The loading amount was 0.035 wt% by this method, and the structure of active sites remained. It is noted that the kind of solvent played an important role in both the modification and catalysis process.

Characterization of single-site catalysts supported by MOFs

It is of great importance to develop advanced characterization techniques to identify the accurate composites and chemical environments of single-site catalysts supported by MOFs. Generally, the atomic structure of single ions or clusters can be distinguished by aberration-corrected high-angle annular dark-field scanning transmission electron microscopy (HAADF-STEM) [101]. And the elemental distribution can be identified by energy-dispersive X-ray spectroscopy (EDX). However, they just provide the localized microstructural information.

Unlike other supports, MOFs are porous crystal materials with ambiguous structure and the processes for grafting single-site catalysts are often through a single crystal-to-single crystal (SCSC) fashion, making the determination of exact structure of single-site catalysts by single crystal X-ray diffraction (SCXRD) feasible. The precise characterization of active sites would drive generation of new catalysts. Pardo et al. reported that isolated single Fe^{III}-O sites were hosted in $Ni^{II}_2(Ni^{II}_4(Cu^{II}_2(Me_3mpba)_2)_3)\cdot 54H_2O$ by means of cation exchange with Ni ions and the exact structure was determined by SCXRD, confirming the nature of the Fe^{III} active site in the hydrogenation of acetylene reaction [43]. Further, translation of the active site concept to even more robust and inexpensive titania and zirconia supports. As for the MOFs with mixed ligands incomplete modification of active sites, the intrinsic disorders make SCXRD not work. There are alternative characterization methods like DRIFTS and XAS to identify the structure of active sites.

Diffuse reflectance infrared Fourier transform spectroscopy (DRIFTS) can detect the evolution of functional group in the modification and reaction process. Especially for the various hydroxyl groups on the nodes, with the weakened intensity or disappearance of particular peak after modification, the location of single-site catalysts on the nodes can be identified. Further with CO as a probe molecule, the CO-DRIFTS can provide more information about the structure and chemical environment of molecular fragments. The value of ν_{CO} can distinguish the adsorption mode of single-site catalysts supported by MOFs (chemisorption or physisorption) and its frequency shifts with the state change of the active sites can be investigated by *in situ* characterization. The value of ν_{CO} changes with the binding modes of CO on the metal sites. Dicarbonyl species are formed on mononuclear metal cations, whereas on multinuclear ones or clusters, CO binds in both atop and bridged configurations, based on which the species of metal center can be determined. The sharpness or full width at half-maximum (fwhm) values of ν_{CO} bands demonstrate uniform distribution of single-site catalysts, which facilitates the structure definition and selectivity improvement. Gates *et al.* applied the DRIFT for characterization of Ir complex in UiO-66 [65]. There are only one kind hydroxyl groups, μ_3-OH characterized by IR bands at 3674 and 3644 cm^{-1}, on the node of perfect UiO-66. However, there are lots of defects caused by linker missing in UiO-66 and missing linker sites on Zr_6 nodes are occupied by two OH terminal hydroxyl groups, in which the IR band intensities are at 3780 and 3692 cm^{-1}. After supporting $Ir(C_2H_4)_2$, the intensity of the 3692 cm^{-1} band decreased significantly, and the 3780 cm^{-1} band disappeared, and the intensities of μ_3-OH groups remained, demonstrating that the Ir complexes are isolated on these defective sites rather than μ_3-OH sites on the nodes. There is a concomitant growth of ν_{CO} bands at 2074 and 1996 cm^{-1}, indicating that chemisorbed iridium *gem*-dicarbonyls are mononuclear [121]. And the high degree of uniformity of Ir sites in UiO-66 is confirmed by the small fwhm values in ν_{CO} band of gem-dicarbonyls of iridium, which is smaller than that on ZrO_2. With the DRIFT, the adsorption peaks of anchoring sites on the ligands can give more detailed information. For example, in the synthesis of ANL1, the O—H vibration at 3583 cm^{-1} existed, meaning the auto deprotection of hydroxyl groups [111]. The attenuation of the peak after loading $Ti(O^iPr)_4$ and retention of the peak of hydroxyl groups on the nodes at 3673 cm^{-1} demonstrated the successful incorporation of $Ti(O^iPr)_2$ on the ligands.

Another alternative method is X-ray absorption spectroscopy (XAS) that can provide electronic and structural information of the active sites such as oxidation states from X-ray absorption near edge spectroscopy (XANES) and coordination numbers, and coordination configurations from the extended X-ray absorption fine-structure (EXAFS) measurement. For example, single CoCl sites were anchored on the nodes of UiO-68, however, the crystallographic disorder made the Co coordination environments in UiO-CoCl fail to be established by X-ray crystallography [6]. Fitting EXAFS regions of UiO-CoCl confirmed that the Co centers were coordinated to three SBU oxygen atoms and one halogen atom. By comparing the energies of the pre-edge peaks to the Co(II) reference compounds, the oxidation states of UiO-CoCl are determined as +2. In addition, single-site catalysts anchored on the ligands share the same methods. Like $IrCl_3$ supported on the ligand of mbpyOH-UiO in the DMF/THF mixed solutions, the local coordination environments of Ir in MOFs were deduced from X-ray absorption spectroscopy (XAS) at the Ir L_{III}-edge [97]. XANES of mbpyOH-$IrCl_3$-UiO confirmed the oxidation state of Ir^{3+} by a rising edge similar to $IrCl_3$. Fittings of the EXAFS regions afforded six-coordinated Ir centers with three chlorides atoms, two nitrogen atoms from bipyridine moiety, and one oxygen atom from a THF molecule in the first coordination sphere.

Altogether, the electron microscopy with high resolution can show the distribution of single-site catalysts and elemental composition directly, however, it can only provide localized microstructural information. The exact structure of single-site catalysts supported by MOFs can be determined by SCXRD. As for some active sites with crystallographic disorder, they can be deduced by DRIFT and XAS. The DRIFT with a probe molecule CO is a simple method to provide approximate information about the location, uniformity, adsorption mode and composition of single-site catalysts. and the XAS offers an alternative method to characterize the electronic and structural information. With these characterization techniques, the precise structure and chemical environment of the single-site catalysts can be determined, which facilitates the research of reaction mechanism and structure-activity relationships.

Isolated single-sites catalysts supported by MOFs for catalysis

MOFs as supports for enhancing the single-site catalysts' performances

Comparing with traditional solid supports

Single-site catalysts supported by MOFs could exhibit the significantly improved performances compared with the traditional supports. For examples, molybdenum (VI) species are catalytically active in the synthesis of epoxides but suffer from deactivation by μ-oxo oligomerization in homogeneous reactions. Furthermore, traditional supports like silica and alumina fail to fix them onto their surfaces. This challenging problem was solved by confining the single molybdenum sites on the nodes of NU-1000 (Mo-SIM) via solvothermal deposition method, which could suppress the deacti-

vation of active sites [62]. Extended X-ray absorption fine structure (EXAFs) measurement indicated that Mo-O and Mo-O-Zr were formed, and Mo species were monometic or at most few Mo atom clusters. A very low yield of 5% was obtained after 7 h for pure NU-1000, while Mo-NU-1000(SIM) exhibited a high conversion rate of ~93% with a high selectivity of ~99% for cyclohexene epoxide and the ring-opened diol. These indicated that the catalytic activity was solely attributed to the deposited molybdenum species. In addition, Mo-ZrO_2 displayed a yield of 97% with a selectivity of 99%, but significant leaching of the catalytic species was found and the yield was decreased to 30% at the third cycle. As for Mo-NU-1000(SIM), no deactivation was explored within three cycles, demonstrating exceptional stability of molybdenum(VI) oxide deposited on Zr_6 nodes in NU-1000.

The strong Lewis acidic Nd oxide sites are active in alkene epoxidation. For example, Farha et al. successfully grafted Nb(V) oxide sites onto the nodes of NU-1000 via atomic layer deposition (AIM) and solution-phase grafting (SIM) [82]. The Nb(V) content in MOF-supported catalysts (1.6 mmol/g for AIM vs. 1.4 mmol/g for SIM) was approximately an order of magnitude higher than that on ZrO_2 (0.19 mmol/g), since commercial ZrO_2 has a significantly lower density of grafting sites when compared to NU-1000. Difference envelope density measurements indicated that using the two synthetic methods resulted in different local structures of Nb(V) ions within NU-1000. Deposited Nb(V) atoms in Nb-AIM were uniformly distributed in the lateral cavities between the two adjacent Zr_6 nodes along the *c*-axis. By contrast, solution-phase grafting resulted in deposition in the same cavities, but with a bilobal distribution of electron density, suggesting formation of Nb oxide dimers. The catalytic performance of Nb-NU-1000 was investigated for catalytic cyclohexene oxidation in respect with Nb-ZrO_2 and Nb-SiO_2 samples. ZrO_2 gave exclusively oxidation products that originated from radical decomposition of H_2O_2, whereas bare NU-1000 was selective to direct cyclohexene oxidation with low yield. Nb-NU-1000 catalysts showed high pathway selectivity, *e.g.* 72% for AIM, and 88% for SIM, while Nb-ZrO_2 had a pathway selectivity of 45%, indicating that the Nb(V) sites were responsible for direct cyclohexene epoxidation.

The Mn^{IV}-oxo species in high-spin state are efficient oxygen atom transfer (OAT) reagents in oxidation reactions. This highly active species are stabilized by relatively weak ligand fields provided by SBU of MOF-5 and the site-isolated environment provided by the framework could enhance the lifetime of the high-valence intermediate by preventing dimerization or other deactivating reactions [35]. Farha et al. carried out metalation of the Zr_6 nodes of NU-1000 by installing Co(II) ions, in which the readily accessible $-OH/-OH_2$ groups on Zr_6 nodes behaved as site-isolating grafting sites to control the position of deposited metal ions, via solvothermal deposition method and atomic layer deposition method, denoted as Co-NU-1000(SIM) and Co-NU-1000(AIM) [59]. The catalytic performance of both catalysts for oxidative dehydrogenation (ODH) of propane was tested under steady-state condition with a flow of propane and O_2 at a molar ratio of 6 to 5 in contrast with Co(II) on commercial ZrO_2. The result indicated that the obtained products were the mixture of propene and CO_2. As for Co-NU-1000(AIM), the turnover frequency (TOF) was determined to be 1.02 h^{-1} on a per cobalt atom basis at 230 °C, while it was 0.54 h^{-1} for Co-NU-1000(SIM). The possible reason for difference in catalytic activity was ascribed to a new Co···Co interaction in Co-NU-1000(AIM) upon activation in O_2 at 230 °C, which was absent in Co-NU-1000(SIM). In contrast, TOF value was determined to be only 0.15 h^{-1} on a per cobalt atom basis at 230 °C for 10 wt% Co/ZrO_2, demonstrating advantages of using Zr_6 nodes of NU-1000 as the catalyst support. Furthermore, both Co-NU-1000(SIM) and Co-NU-1000(AIM) exhibited the excellent stability, that is, after 24 h time on stream, propane conversion was kept around 8.7% for Co-NU-1000(AIM) and about 3.8% for Co-NU-1000(SIM). Similarly, Farha et al. also introduced Ni ion for metaltion of Zr_6 nodes via atomic layer deposition method, denoted as Ni-NU-1000(AIM) [77]. When used as catalyst for hydrogenation of ethylene to ethane, Ni-NU-1000(AIM) showed a TOF value of 0.9 s^{-1} on a per nickel atom basis. As contrast, Ni-ZrO_2 had an initial TOF value of 0.6 s^{-1}, but deactivated quickly. Remarkably, Ni-NU-1000(AIM) was highly stable and the conversion rate was kept ~100% for 2 weeks without deactivation.

Zeolites, inorganic crystalline porous materials, possess pronounced thermal and hydrothermal stability and can stand under harsh reaction conditions [122]. With small pore size (less than 1 nm), shape-selective reactions can be performed. However, the number of single-site catalysts that can be introduced is limited by the small pore volume, which consequently restricts the strength of active sites formed on zeolites. Compared to these materials, MOFs shows great advantage with high surface area, tunable pore size and pore environment. And, MOFs provide a great opportunity to rationally design the active site and the microenvironment with an unprecedented degree of precision [123]. For example, single Cr^{3+} sites anchored on the linkers of UiO-66-CAT were an efficient and "green" alcohol oxidation catalyst for a range of substrates [112]. The UiO-66-CrCAT could quantitative oxidize benzylic alcohols in 12 h using 1.1 equiv of TBHP as an oxidant and chlorobenzene as the solvent at 70 °C. However, a Cr-exchanged zeolite catalyst gave yields of 79–95% with benzylic alcohols but required 4 equiv of TBHP [124]. Moreover, UiO-66-CrCAT shows no leaching of Cr, while the Cr-containing zeolites were often susceptible to solvolysis by polar solvents and extensive leaching of the metal species.

The mesoporous silica materials possess large pore size (2–50 nm) while zeolites rarely have pore size larger than 1 nm without a significant loss in stability. MOFs with pore size from 0.5 nm to 9.8 nm may bridge the gap and can be designed for various applications [122]. With tunable pore size, MOFs could isolate only one catalyst molecular per pore to protect them from dimerization and leaching, such as MnTD encapsulated by MIL-101 [119]. The MnTD could also be incorporated in the large pores of FDU-12 with a diameter of 18.6 nm and more than one catalyst molecules were incorporated per pore. However, in the reaction of water oxidation, the rate of MnTD@FDU-12 was found to be only one fourth compared to that with MnTD@MIL-101. And the lifetime of MnTD@FDU-12 in reactions was less than 7 h, while the MnTD@MIL-101 could last more than 7 days, which demonstrated the advantage of MOFs' tunable pores in the isolation of single-site catalysts.

Comparing with homogeneous counterpart

The homogenous catalysts can be introduced into MOFs with the preservation of intact structure. The heterogenization of homogenous catalysts endows it with good recyclability. More importantly, most single-site catalysts can be isolated in MOFs without the protection of bulky, elaborately designed ligands. Thus, the active site isolation protects catalysts from forming inactive dimers or oligomers, which makes them more stable and active than the homogenous counterpart in catalytic reactions. For examples, Lin *et al.* introduced the monophosphine-ligated metal center (Ir and Rh) in MOFs to prevent deleterious disproportionation reactions/ligand exchanges. The single-site catalysts in MOFs showed the high activity in hydrosilylation of ketones and alkenes, the hydrogenation of alkenes, and the C–H borylation of arenes, while the homogenous counterpart has negligible activity [104]. Single $(bpy)Co(THF)_2$ sites fixed on the linker of UiO-867 are highly active in alkene hydrogenation with high turnover numbers of 2.5×10^6 [93]. However, the homogeneous counterparts $Co(Me_2bpy)Cl_2$ is catalytically inactive due to intermolecular decomposition from inadequate steric protection around the metal

centers. Single Fe^{2+}/Co^{2+}-salicylaldimine site was introduced in UiO-68-NH_2 [107]. After activated by $NaEt_3BH$ in THF, both of them enabled highly active for olefin hydrogenation and achieved turnover numbers of up to 145,000 with good recyclability for more than 15 times. As contrast, the homogenous complexes were totally inactive in reactions due to the intrinsic instability with low-coordination-number and formation of tetrameric species with the formula of $Fe_4(sal)_4Cl_4(THF)_2$, which was prohibited by isolation in MOFs.

Nanostructured MOFs as supports

MOFs with advanced nanostructures like hollow or two-dimesional (2D) MOFs can further enhance the catalytic performance by facilitating diffusion of substrates and products [125,126]. For examples, Wang et al. designed and synthesized Zr-porphyrin hollow MOF with high surface area and low density. By tuning the crystal nucleation and growth in the H_2O and benzoic acid solution, the hollow MOFs are generated and could catalyze hydrogen evolution reactions under visible-light irradiation after loading Ir/Pt catalysts [103]. Ir and Pt sites are introduced in MOFs easily by solvothermal method and have a synergic effect in the photocatalytic HER, in which porphyrin-Ir units and porphyrin-Pt units act as photosensitizer and catalyst, respectively. At the same time, the MOFs facilitate separation of charge carriers and the charge-transfer resistance reduction. And the uncoordinated porphyrin can rebind with leaching ions. All these boost the performance of the MOF complex. The H_2-generation rate reached up to 201.9 mmol g^{-1} h^{-1} and the activity was kept after 3 cycles. Compared with the bulk MOFs, the hollow MOFs shows 6 times higher H_2-generation rate, demonstrating the advantage of hollow morphology in mass transportation [19]. Wang et al. synthesized a Hf-BTB 2D MOFs, in which six of the connection sites on the cluster $[Hf_6(\mu_3\text{-}O)_4(\mu_3\text{-}OH)_4]$ were protected by formate groups, leaving the remaining six in the same plane to connect to the benzene-1,3,5-tribenzoate (BTB) moieties [100]. Part of ligands, benzene-1,3,5-tribenzoate, were exchanged with 4′-(4-benzoate)-(2,2′,2″-terpyridine)-5,5″-dicarboxylate (TPY) to isolate single Fe sites (Fe-TPY-MOL) and the structure remained intact. After activation with $NaBHEt_3$, Fe-TPY-MOL was capable of efficiently catalyzing the hydrosilylation of styrene to afford the pure anti-Markovnikov product. As contrast, the activity of 3D stacked version of the composites decreased 70% and the 3D interlocked one was totally inactive, which was attributed to the limited mass transportation in the channels of MOFs. The homogenous catalysts exhibited the lower activity and Markovnikov product due to formation of Fe^0 nanoparticles from decomposition. These demonstrated the merit of MOLs in isolation of single-site catalysts with less limited mass transportation.

Single-site catalysts supported by MOFs possessing their own unique properties

Selectivity is an important factor for evaluating the performance of single-site catalysts. With uniform nanopore size, rigid structure, and various binding motifs on the linkers and SBUs, single-site catalysts confined in MOFs could exhibit the distinct activity and selectivity in heterogeneous catalysis together. The polydispersity indices and molecular weight of products in polymerization reaction could be controlled very well by the uniform active sites. Dincă et al. incorporated different transition metal ions (Ti, Cr, Fe, Co and Ni) in MFU-4*l* via cation exchange. Due to the uniform single catalytic sites, the Cr- and Ti-MFU-4*l* showed high activity towards polymerization of ethylene and copolymerization of ethylene and propylene with low polydispersity indices and good molecular weight control. The polydispersity indices derived by HT-GPC are generally low, ranging from 5 for Cr(III)-MFU-4*l* to 2.0 for Ti(IV)-MFU-4*l* at 40 bar of ethylene. These PDI values are considerably lower than those reported for polyethylene produced from molecular scorpionate complexes chromium [72]. Moreover, they could exhibit high selectivity by effectively precluding multi active sites reaction pathway via controlling the nanopore structure. The complexes, $(bpy)Re(CO)_3Cl$, can catalyze the photochemical reduction of carbon dioxide via two reaction pathways, unimolecular and bimolecular intermediate, in the homogenous reactions at the same time. However, after anchored on the linkers of UiO-67-bpy, only the unimolecular pathway is permitted with a higher activity because of isolation of active sites in UiOs compared with the homogenous counterpart [96]. Also, few complexes isolated solid supports are trans conformation and this can be realized in MOFs. Zhou et al. reported that trans-coordinated metal complexes could be anchored in PCN-160 with exposed equatorial position by SALE [127]. Part linkers of PCN-160 can be replaced by 4-carboxybenzylidene-4-aminobenzate, which would dissociate and create linkers missing

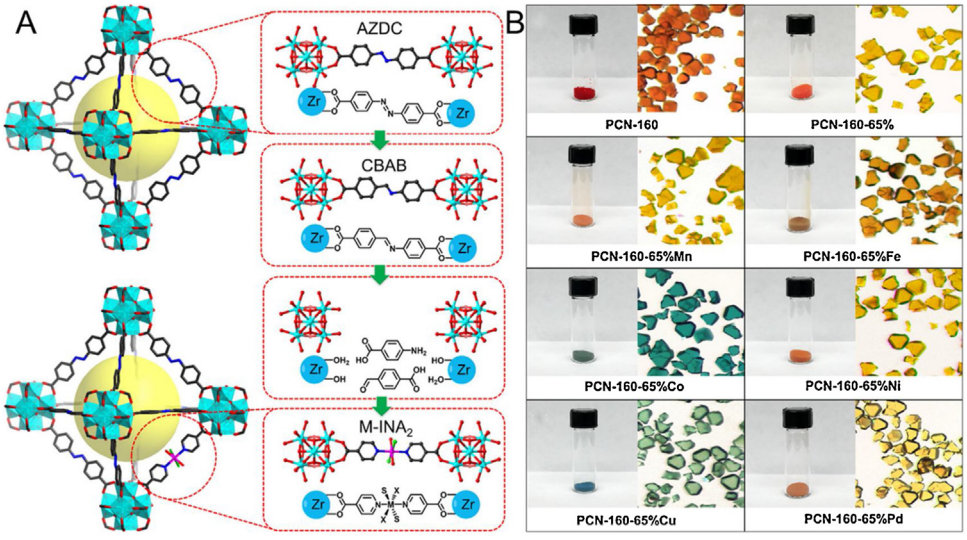

Fig. 9. (A) Structure of PCN-160 and PCN-160-R%M with *trans*-chelating ligands and transformation of ligand fragment in PCN-160 by CBAB exchange, linker labialization, and installation of M-INA2. These figures are based on respective single-crystal structures after removal of the disordered fragments. (B) Photos and microscope images of PCN-160, PCN-160-65%, and PCN-160-65%M (M = Mn, Fe, Co, Ni, Cu, and Pd). Reprinted with permission from Ref. [127] Copyright (2018) American Chemical Society.

defects. Then Ni-INA_2 (4-Pyridinecarboxylate, INA) or metal INA complexes moieties are incorporated in the defect sites. Due to more sterically accessibility, the catalytic activity of PCN-160-47%Ni in ethylene dimerization reaction is $\tilde{7}$ times higher than the cis-coordinated Ni in UiO-67-50%Ni (Fig. 9). Charge separation is used to enhance the Lewis acidity of active sites inside MOFs. With the octatopic ligand TBCPPP (tetrakis-3,5-bis((4-carboxy)-phenyl)phenyl-porphyrin) chelated with $Mn^{III}Cl$ (or $Fe^{III}Cl$ ions) and anionic $[In(CO_2)_4]^-$ SBUs, UNLPF-13-$Mn^{III}Cl$ is produced by solvothermal reactions with Cl^- coordinated to Mn^{III} strongly and UNLPF-14-Mn^{III} with no extra anions coordinated to Mn^{III} is produced with TBCPPP-$Mn^{III}[BF_4]$, in which charge is balanced with $[In(CO_2)_4]^-$. As a comparison of coordination intense, PCN-223-$Mn^{III}[SbF_6]$ is synthesized. In the cyclo isomerization of 1,6-enynes reactions that can be catalyzed by Mn^{III}-porphyrin, UNLPF-14-Mn^{III} shows the high reactivity and 95% selectivity to endo product, while both UNLPF-13-$Mn^{III}Cl$ and MnTPPCl have negative reactivity. And PCN-223-$Mn^{III}[SbF_6]$ performs moderate activity and selectivity due to the weekly coordinated SbF_6^-. The different selectivity and activity among the three catalysts are ascribed to the coordination intense, highlighting the essential role of the complete charge separation and the advantage of zwitterionic MOFs. Furthermore, the electronic properties of catalysts supported by MOFs can be tuned easily, which can act as the only factor to explore the relationships between structure and properties [128,129]. The single CoH sites were anchored on the nodes of MIL-125(Ti), $Ti^{IV}{}_8(\mu_2\text{-}O)_8(\mu_2\text{-}OH)_4$ [41]. After reduced into $Ti^{III}{}_2Ti^{IV}{}_6$-BDC-CoH, the single CoH sites can catalyze hydrogenation of arene with high turnover number (TON) values of 10,526 and possess size-exclusion effect due to the uniform shape and size of MOF channels. However, the $Ti^{IV}{}_8$-BDC-CoH is totally inactive, indicating the pivotal role of electronic effect of supports in tuning catalysts.

Synergistic catalysis achieved by single-site catalysts supported by MOFs

Structural regularity and synthetic tenability of MOFs allow hierarchical integration of multiple functional moieties, and different parts can cooperate with each other for achieving the improved performances [130–133]. It is noted that photosensitizers are necessary in photoreactions to facilitate light-harvesting. The photosensitizers (PSs) and catalytic centers can be incorporated in MOFs to facilitate multielectron or radical transfer in photoreactions. $[Ru(dcbpy)(bpy)_2]^{2+}$, an effective molecular photosensitizer, and $CoCl_2$ were introduced in UiO-67-bpy and the obtained composite showed high activity for light-driven H_2 production. The catalysts could achieve 27,853 mol H_2/g of MOF after 40 h, accounting for TON of 99 based on Co [98]. With the *in situ* X-ray absorption spectroscopy, the enhancement is elucidated that the intermediate species, Co^+, is formed by electron transition from Ru PS to Co sites, and is long-lived due to the efficient charge separation by Ru moiety. With multi components, photoredox and organometallic dual catalyst, the cross-coupling reactions between aryl iodides and aryl thiols under visible light can be realized [134]. The Ir and Ni complexes are incorporated into UiO-69-bpy, which could act as photoredox catalysts to generate radicals and electrons and facilitate the cross-coupling reactions, respectively (Fig. 10). Due to the close sites between Ir and Ni, which facilitates both electron and thiophenol radical transfer, TON could reach 35,800 and the catalytic performance is much better than its homogenous counterpart. The activity of catalysts was kept well after 6 successive cycles. Lin et al. assembled a 2D MOF (Hf_{12}-Ru) with bis(2,2′-bipyridine)[5,5′-di(4-carboxylphenyl)-2,2′-bipyridine]ruthenium(II) dichloride and $HfCl_4$ [130]. Replacing the trifluoroacetic acid coordinated on the nodes, 2-(5′-methyl-[2,2′-bipyridine]-5-yl)acetic acid (H-MBA) ligands can apply as binding sites to afford $Re(CO)_5Cl$ or $Mn(CO)_5Br$ catalysts with a thickness of 3.7 nm. In the composites, every active site is adjacent to six photosensitizer molecules and the distance between them is just 1–2 nm, which makes multielectron transfer process easier. Due to the well-designed structure, the catalysts exhibit the reduction of carbon dioxide with turnover numbers of 670 even under sunlight. Cohen et al. designed DMOF with $Zn(NO_3)_2$ and mixed ligands, 2-phenylpyridine-5,4′-dicarboxylic acid (dcppy) and 1,4-Diazabicyclo[2.2.2]octane (dabco) [135]. $[Ir(COD)(OCH_3)]_2$ (COD = 1,5-cyclooctadiene) was anchored on the dcppy ligands by cycle metalation postsynthetic modification methods. The composites are capable of catalyzing Meinwald rearrangement reaction, the allylic N-alkylation of indoline. Further, they introduced dcppy ligands cycle metalated with $[Ir(COD)(OCH_3)]_2$ to IRMOF-9 [136]. Together with amino groups on H_2bpdc-$(NH_2)_2$ ligands, the composites are able to catalyze tandem Meinwald rearrangement-Knoevenagel condensation reaction in one pot. This tandem reaction can't be realized by the two active sites in homogenous reactions because of alkylation of the amine functionality by the Ir site. These demonstrate the merits of site isolation by MOFs.

Function synergy between single sites and supports together with nanopore confinement effect

Single-site catalysts supported by MOFs could achieve size-dependent selective catalysis, and thus it is of great significance to introduce MOFs with tunable nanopore structures as supports. For examples, the molecules with larger size are excluded passing through or generated in the nanopores, which endows the active sites with unexpected selectivity due to the uniform shape and size of channels of MOFs. Borylation of methane remains a vital goal in the chemical sciences due to its vast reserves and low intrinsic reactivity. A major challenge in this regard is selective borylation towards the monoborylated product that is more active than methane and can easily lead to over-functionalization. Farha et al. took advantage of the uniform nanopore size of MOFs to realize high selectivity towards specific size products despite thermodynamic unfavourability [38]. Single Ir complexes were anchored on ligands (1,10-phenanthroline-3,8-dicarboxylic acid) of UiO-67 which could catalyze methane borylation towards the thermodynamic unfavorable monoborylated product. UiO-67-Mix-Ir(5 mol%) fully converted B_2pin_2 and yielded about 17% of CH_3Bpin with a turnover number (TON) of 32 in cyclohexane at 150 °C and 34 atm of CH_4 for 14 h, which is slightly higher than the homogenous analogue (TON = 23). Remarkably, the chemoselectivity ratio of mono- versus diborylated methane products is 15:1 for the MOF-based heterogeneous catalyst. In dodecane, the catalysts exhibited a chemoselectivity higher than 99% (mono versus bis at 19.5% yield; turnover number = 67) for monoborylated methane. The high selectivity came from the nanopore confinement effect inside MOFs. The aperture size of UiO-67 is 0.8 nm and the largest dimension (vertex to vertex of the octahedron) is close to 1.88 nm which preferred the formation of monoborylated product (0.73×0.88 nm, linear) rather than thermodynamically favored diborylated methane (0.80×1.39 nm, bent) in this reaction (Fig. 11). When 1 equivalent of bulky coordinated tricyclohexyl phosphine per iridium is added to poison the Ir complexes on the MOFs' surface, the selectivity doesn't change with decreased conversion, which corroborates the shape-selective effect of the nanopore structures of MOFs. UiO-67-Mix-Ir deactivates after two catalytic runs while the MOF structure is maintained, which is possibly due to the degradation of the active iridium species. In addition, $Ti(OiPr)_4$ is one kind of active sites for hydroboration of carbonyl compounds. It can be anchored on the biphenol groups in ANL1 and exhibit high reactivity in hydroboration of a wide range of carbonyl compounds with excellent functional group tolerance

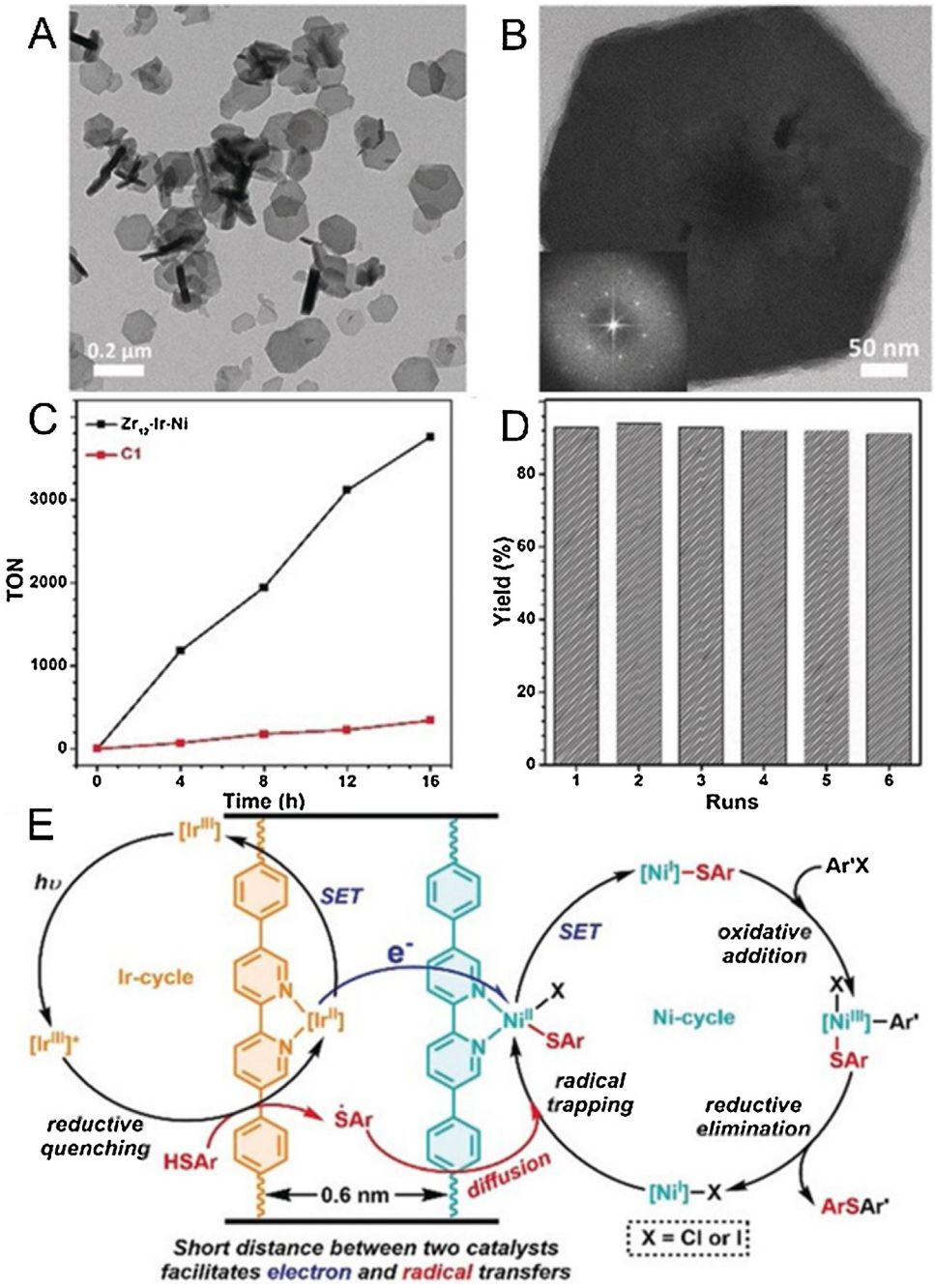

Fig. 10. Synergistic catalysis achieved by different active single sites supported by MOFs. TEM image (A) and HRTEM image and FFT pattern (inset) (B) of Zr_{12}-Ir. (C) Plots of conversion vs. time at 0.02 mol% catalyst loading of Zr_{12}-Ir-Ni and homogeneous catalysts. (D) Plots of yields (%) of products catalyzed by recovered Zr_{12}-Ir-Ni (0.02 mol% catalyst loading) in six consecutive runs. (E) Proposed mechanism for the C–S cross coupling reaction catalyzed by Zr_{12}-Ir-Ni. Reprinted with permission from Ref. [134] Copyright (2018) Wiley-VCH.

[111]. And the single-site catalysts show group selectivity for the hydroboration of aldehyde versus ketone because of the formation of bulkier borate esters that could block the catalytic pore.

Except of extra-large molecules, the well-defined nanopore structure of MOFs can provide another kind of steric hindrance that the narrow space around active sites hinders reagents entering the coordination sphere of the active sites. For example, Lin et al. designed single μ_4-O-CoH sites on the nodes of UiO-68, which is active for catalytic hydrogenation of arange of olefins at room temperature due to the site-isolated, electron-deficient and coordinatively unsaturated chemical environment [6]. However, the μ_3-O-CoH confined in an equilateral triangle with edge length of 4.4 Å surrounded by three phenyl rings provides limited space for hydrogenation of tetrasubstituted olefins and heterocycles. To enlarge the space around active site, a new node $Zr_8(\mu_2\text{-}O)_8(\mu_2\text{-}OH)_4$ is designed, which can provide rhombus space with an edge length of 4.5 Å. In the Zr-MTBC (MTBC, 4′,4‴,4⁗,4⁗′⁗′-methanetetrayltetrakis([1,1′-biphenyl]-4-carboxylic), both Zr_8 nodes and Zr_6 nodes exist with the ratio of 1:3. After modified with single Co-H sites, the Zr-MTBC-CoH is a high active catalyst for hydrogenation of a broad scope of substrates, including highly hindered and inactive alkenes, imines, carbonyls, and heterocycles. The Co-H anchored on the Zr_6 nodes of UiO-68, whose structure is exactly same to that in

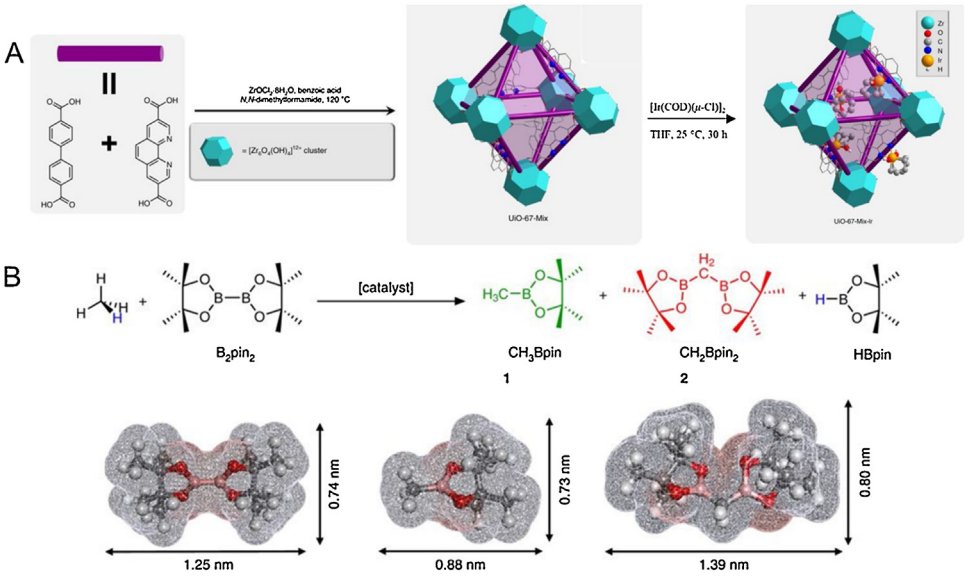

Fig. 11. Size-dependent selective catalysis achieved by single-site catalysts confined in nanopores of MOFs. (A) Synthetic scheme of the catalyst UiO-67-Mix-Ir. (B) Reaction scheme of methane borylation with B_2pin_2. The molecular sizes of 1 and 2 are shown in the ball and stick model with the van der Waals surface in wire mesh. Reprinted with permission from Ref. [38] Copyright 2016, Springer Nature.

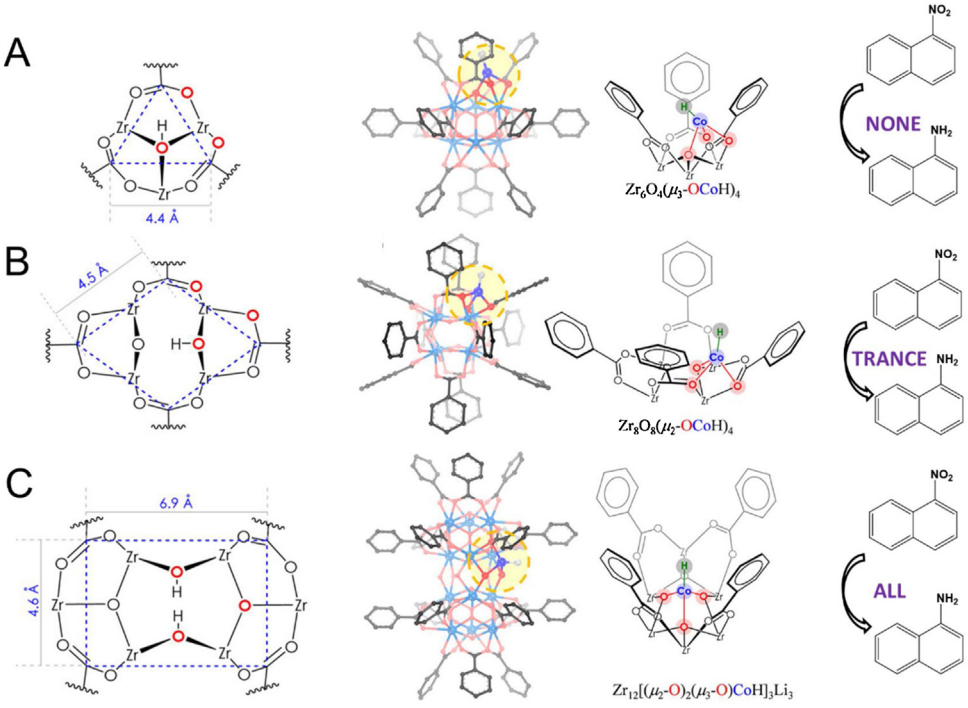

Fig. 12. The effect of localized steric hindrance in nanopores of MOFs. Depiction of three Co catalysts with vastly different activities and selectivities in hydrogenation of nitroarene based on different SBUs of Zr MOFs and the comparison of the electronic and steric properties of Co binding sites in Zr_6-, Zr_8-, and Zr_{12}-SBUs. Reprinted with permission from Ref. [29] Copyright (2017) American Chemical Society.

Zr-MTBC, is inactive in hydrogenation of bulky and rigid trisubstituted alkenes, suggesting that the active sites in Zr-MTBC-CoH are the Co-H site on Zr_8 nodes [36]. Further, a new node $Zr_{12}O_8(\mu_3\text{-}OH)_8(\mu_2\text{-}OH)_6$ is generated from dimerizing two Zr_6 clusters via six μ_2-OH groups by adding a certain amount of water in the reaction mixture of UiO-68. Through a similar modification and activation process, the single Co-H sites are confined in sterically open rectangle space (4.6×6.9 Å) with a different structure, $[(\mu_2\text{-}O^-)_2(\mu_3\text{-}O)CoH]^-$, due to short distance between μ_3-OH and μ_2-OH groups. Thanks to dianionic nature of the binding site, the Co-H center is more electron-rich compared with μ_4-OCoH site on the Zr_6 or Zr_8 nodes, which facilitates hydrogenation of nitroarenes, nitriles, and isocyanides to corresponding amines with excellent activity and selectivity (Fig. 12) [29]. The narrow space around active sites can be implemented to enhance the catalytic performance. Huang *et al.* synthesized a series of isoreticular UiO-67(bpy) with methyl groups at different sites of ligands, which can tune the space around single Pd sites supported on the ligands [137]. After loading $PdCl_2$, the obtained MOFs could catalyze Suzuki-Miyaura cross-coupling reactions, in which the turnover-limiting step of the

Table 1
Summary of synthesis of single-site catalysts isolated in MOFs as well as their applications in heterogeneous catalysis in the reported literatures.

Anchoring sites	Methods	MOFs	Active sites	Reactions	Ref.
Nodes	SALI	Zr-NU-1000	Ni(bpy)	Dimerization of ethylene	[53]
		Cr-MIL-101	$B(C_6F_5)_3$	Reduction of imine; hydrogenation of alkylidene malonate	[56]
			V(CAT)	Oxidation of organo-sulfide	[55]
	Cation exchange	Zn-MFU-4*l*	Ti	Polymerization of ethylene; copolymerization of ethylene and propylene; polymerization of 1,3-butadiene	[72,74]
			Cr	Polymerization of ethylene; copolymerization of ethylene and propylene; polymerization of 1,3-butadiene	[72,74]
			Fe	Polymerization of 1,3-butadiene	[74]
			Co	Polymerization of 1,3-butadiene	[74]
			Ni	Polymerization of 1,3-butadiene	[74]
			V	Polymerization of ethylene	[75]
	Free hydroxyl groups as anchoring sites	Zn-MOF-5	Mn	Olefin epoxidation	[35]
		Ti-MIL-125	CoCl	Hydrogenation of areneand heteroarene	[41]
		Zr-UiO-68	CoCl	Benzylic C-H borylation; benzylic C–H silylation; hydrogenation of olefins	[6]
			FeBr	sp^3 C–H amination	[6]
		Zr-MTBC	CoCl	Hydrogenation of alkenes, imines and carbonyls heterocycles	[36]
		Zr_{12}-TPDC	CoCl	Hydrogenation of nitroarenes, nitrilesand isocyanides	[29]
		Hf-MOF-808	V	Alcohol oxidation	[13]
		Zr-UiO-66	V	Oxidative dehydrogenation of cyclohexene	[64]
			Al	Meerwein–Ponndorf–Verley	[138]
			$Ir(CO)_2$	Ethylene hydrogenation; ethylene dimerization	[65]
		Zr-UiO-69-NO_2	MgMe	Hydroboration of ketones, aldehydes and imines; hydroamination of aminoalkenes	[10]
		Cr-MIL-101	$B(C_6F_5)_3$	Reduction of imine; hydrogenation of alkylidene malonate	[56]
			V(CAT)	Oxidation of organo-sulfide	[55]
		Al-DUT-5	Al	Meerwein–Ponndorf–Verley	[138]
			V	Alcohol oxidation	[13]
		Zr-NU-1000	MoS_X	Electrocatalytic hydrogen evolution	[139]
			$(py_3tren)AlCo$	Oxidation of benzyl alcohol	[66]
			$(py_3tren)RhGa$	Selective semihydrogenation of alkynes	[67]
			Mo	Cyclohexene epoxidation	[62]
			Co	Oxidative dehydrogenation of propane	[59]
			Nb	Epoxidation of alkene	[82]
		Hf-NU-1000	ZrBn	Stereoregular1-hexene polymerization	[61]
			Co	Oxidative dehydrogenation of propane	[59]
			Pt	Hydrogenation of ethylene	[79]
	AIM	Zr-NU-1000	$Ir(CO)_2$	Hydrogenation of ethylene	[81]
			Nb	Epoxidation of alkene	[82]
			Ni	Light alkene oligomerization	[77,80,140]
			$CoCl_2$ & Ru(bpy)	Photocatalytic H_2 evolution	[98]
			$CuBr_2$	Oxidation of cyclooctene	[95]
		Zr-UiO-67(bpy)	$PdCl_2$	Suzuki–Miyaura cross-coupling	[137]
			$Ir(OH)_2(H_2O)_2$	Hydrogenation of carbon dioxide	[97]
			$Ir(COD)(OH)_2$	Borylation of methane	[38]
			$Re(CO)_5Cl$	Photocatalytic CO_2 reduction	[96]
		Zr-UiO-69	$Ru(bpy)_3$ & $Re(CO)_5Cl$	Photocatalytic CO_2 reduction	[130]
			$Ru(bpy)_3$ & $Mn(CO)_5Br$	Photocatalytic CO_2 reduction	[130]
			$Ir(dF(CF_3)\text{-}ppy)_2(DBB)$ & $NiCl_2$	Cross-coupling of aryl Iodide and thiophenol	[134]
	Pre-modifying linker with anchoring sites	Zr-MPT-MOF	$CoCl_2$	Hydrogenation of olefins, ketones and aldehydes; hydroboration of alkenes; borylation of arenes	[93]
		Hf-TPY-MOL	Fe	Hydrosilylation of terminal olefins	[100]
		Ho-MOF	$PdCl_2$	Heck reaction; Suzuki reaction	[99]
		Zr-UiO-68-sal	Fe	Hydrogenation of olefins	[107]
		Zr-E_2-MOF	RhCl	Asymmetric 1,2-addition of aldimine; asymmetric 1,4-additions of arylboronic acids	[141]
Ligands		Zr-PCN-222	$IrCl_2$ & $PtCl_2$	Photocatalytic H_2 evolution	[103]
		Al-TCPP	Pt	Photocatalytic H_2 evolution	[101]
		In-UNLPF	Mn	[2 + 1] Cycloisomerization of enynes; [3 + 2] cycloaddition of aziridines and alkenes	[142]
		In-UNLPF	Fe	[4 + 2] Hetero-Diels–Alder cycloaddition of aldehydes with dienes	[142]
		Co-PCM-101	AuCl	Hydroaddition of 4-pentyn-1-ol	[105]
		Co-PCM-101	CuBr	Hydroaddition of 4-pentyn-1-ol	[105]
		Cr-MIL-101	$Ir(cod)(PCy_3)(py)$	Hydrogenation of alkenes and olefinic alcohols	[106]
		Zr-P_1-MOF	RhCl(nbd)	Hydrosilylation of carbonyls and alkenes; hydrogenation of alkenes	[104]

Table 1 (*Continued*)

Anchoring sites	Methods	MOFs	Active sites	Reactions	Ref.
Nanopores	SALE	Zr-P_1-MOF	Ir(OMe)(cod)	Borylation of arenes	[104]
		Zr-UiO-66	Cr(CAT)	Oxidation of secondary alcohols	[112]
			Pd(TCAT)	Regioselective functionalization of sp^2C–H bond	[113]
		Zr-UiO-67(bpy)	Cp*Rh	Photocatalytic CO_2 reduction	[114]
		Zr-PCN-160	Ni-INA_2	Ethylene dimerization	[127]
	PSD	Zr-UiO-67	ANL1-Ti(O^iPr)$_2$	Hydroboration of aldehydesand ketones	[111]
		Zr-UiO-66	Cr(CAT)	Oxidation of secondary alcohols	[112]
		Al-MIL-53	Pd(Mal)	Heck-type C-C coupling	[108]
	PSM	Cr-MIL-101	Ru(tpy)Cl_3	Oxidation of alcohols	[92]
			Co(dmgH)$_2$(4-HEP)Cl	Photocatalytic H_2 evolution	[110]
			Fe(NacNac)	Intramolecular C–H amination	[109]
		Zr-UiO-69-NH_2	Cu(NacNac)	Amination of cyclohexene	[109]
			Co(NacNac)	Hydrogenation of alkenes	[109]
		Cr-MIL-101	MnTD	Water oxidation	[119]
		Cu-HKUST-1	Fe_4SP	H_2O_2 degradation	[117]
		Zr-UiO-66	(tBuPNP)Ru(CO)-HCl	CO_2 Hydrogenation	[120]
		Zr-NU-1000	$H_3PW_{12}O_{40}$	*o*-Xylene isomerization and disproportionation	[39]

catalytic cycle was reductive elimination and the sterically congested metal centers were favored. In spite of minor BET surface area and similar electronic character of single Pd site, the m-6,6′-Me_2bpy-MOF-$PdCl_2$ exhibited 110- and 496-fold enhancements in activity compared to nonfunctionalized m-bpy-MOF-$PdCl_2$ and m-4,4′-Me_2bpy-MOFPd-Cl_2, respectively.

Moreover, the chemical environment of nanopores can be designed to promote the catalytic performance. Crabtree's catalyst is one of the best commercially available homogeneous catalysts for hydrogenation of alkenes. It can be incorporated in the MIL-101(Cr) by cation exchange with Na^+ salt of sulfonated linkers [106]. In the hydrogeneration of olefinic alcohols, the MOFs composites show enhanced activity due to hydrophilicity derived from the presence of H-bond accepting sulfonate groups as well as Lewis acidic Cr^{3+} sites and Na^+ cations and higher selectivity to hydrogenation against isomerization attribute to interactions between the hydroxyl group of the olefinic alcohols and sulfonate anion. Spatial isolation inside nanopores and reversible coordination of the sulfonate anion make the composites very stable and reusable easily.

Conclusion and perspective

We have summarized the recent progresses in controllable synthesis of isolated single-site catalysts supported by MOFs as well as their distinct catalytic performances (Table 1). With the rapid development of synthesis chemistry, MOFs supported single-site catalysts have been successfully constructed via different strategies and exhibited the excellent catalytic performaces as follows: (1) The highly ordered arrangements of the organic linkers and metal nodes as well as the well-defined nanopore structures of MOFs make them as ideal substrates to support atomically dispersed metal sites located in the metal nodes, linkers and nanopores without protection by bulky, elaborately designed ligands. The catalytic sites can be placed in the well-defined positions of MOFs through either rational design of metal nodes, organic linkers and environments of nanopores or post-synthetic modification. (2) The high surface areas can engender a very high density of catalytic sites, enabling higher chances of contact with substrates and yielding catalysts with high activity and excellent selectivity. (3) The tailorable porosity can provide a special cavity environment for substrates to interact with catalytically active sites, similar conceptually to the secondary interaction spheres of enzyme active sites, which can further enhance activity and selectivity. The integration of the physical properties of inorganic and organic components together with function synergy between MOFs and single-site catalysts provides endless possibility for controllably constructing the desirable catalysts with atomically accurate structures.

However, though tremendous advances have been made, the study on single-site catalysts supported by MOFs is still in its infancy, and many challenges are awaiting to be overcome: (1) The large sized MOFs are currently used as supports for single-site catalysts, which will inhibit the mass transfer and diffusion of substrate and product. (2) The precise control of single-site catalysts inside MOFs is still hard to modulate, and the detailed location position of single-site catalysts is challengeable to realize due to the limited characterization techniques. (3) It is still challengeable to fabricate the single-site catalysts with high metal loading, because single metal ions/atoms tend to diffuse and form large aggregates during catalytic reactions. (4) The collective functions of single-site catalysts and MOFs together with the confinement effect of nanopore structures could exhibit the outstanding performance in respect with conventionl supported catalysts, however, the catalytic mechanism of single-site catalysts is not well understood.

To address above, we suggest the future important research works about single-site catalysts supported by MOFs as follows: (1) It is imperative to develop the novel and effective strategies for synthesis of nanostructured MOFs, and then to construct single-site catalysts with high catalytic efficiency. (2) The mechanism about the heterogeneous nucleation and growth of single-site catalysts on the anchoring sites in MOFs need to be elucidated, and the interfacial interaction between them should be clarified. (3) Smart design of single-site catalysts inside MOFs is to endow them with multifunctional catalytic performances, which will bring new benefits towards significant catalytic reactions. (4) To further realize the catalytic mechanism, it is necessary to develop both *in situ* and *ex situ* characterization techniques along with the theory calculations, which will promote better tuning the catalytic performance of single-site catalysts. All the above will contribute to construction of the single-site catalysts supported by MOFs at molecular level and realization of high catalytic activity, excellent selectivity and long-term stability.

In conclusion, the diverse anchoring sites created inside MOFs have exhibited great potential in supporting single-site catalysts in respect with conventional porous supports, and moreover, the nanopore environment around single-site catalysts could endow them with the excellent activity, selectivity, stability and recyclability, which facilitates the research in reaction mechanism and further applications in various catalytic reactions.

Acknowledgements

This work was supported financially by National Key Basic Research Program of China (2014CB931801 and 2016YFA0200700, Z.Y.T.), National Natural Science Foundation of China (21890381,

21721002 and 21475029, Z.Y.T.; 21722102, 51672053 and 21303029, G.D.L.), Beijing Natural Science Foundation (2182087, G.D.L.), Frontier Science Key Project of Chinese Academy of Sciences (QYZDJ-SSW-SLH038, Z.Y.T.), CAS-CSIRO Cooperative Research Program (GJHZ1503, Z.Y.T.), the project of "K. C. Wong Education Foundation" (Z.Y.T.), and Youth Innovation Promotion Association CAS (2016036, G.D.L.).

References

[1] X. Cui, W. Li, P. Ryabchuk, K. Junge, M. Beller, Nat. Catal. 1 (2018) 385–397.
[2] Z. Li, D. Wang, Y. Wu, Y. Li, Natl. Sci. Rev. 5 (2018) 673–689.
[3] X.-F. Yang, A. Wang, B. Qiao, J. Li, J. Liu, T. Zhang, Acc. Chem. Res. 46 (2013) 1740–1748.
[4] G. Kyriakou, M.B. Boucher, A.D. Jewell, E.A. Lewis, T.J. Lawton, A.E. Baber, et al., Science 335 (2012) 1209–1212.
[5] J.M. Thomas, R. Raja, D.W. Lewis, Angew. Chem. Int. Ed. 44 (2005) 6456–6482.
[6] K. Manna, P. Ji, Z. Lin, F.X. Greene, A. Urban, N.C. Thacker, et al., Nat. Commun. 7 (2016) 12610.
[7] J.M. Thomas, Phys. Chem. Chem. Phys. 16 (2014) 7647–7661.
[8] C. Copéret, A. Comas-Vives, M.P. Conley, D.P. Estes, A. Fedorov, V. Mougel, et al., Chem. Rev. 116 (2016) 323–421.
[9] J.D.A. Pelletier, J.-M. Basset, Acc. Chem. Res. 49 (2016) 664–677.
[10] K. Manna, P. Ji, F.X. Greene, W. Lin, J. Am. Chem. Soc. 138 (2016) 7488–7491.
[11] C.Y. Tang, W. Smith, D. Vidovic, A.L. Thompson, A.B. Chaplin, S. Aldridge, Organometallics 28 (2009) 3059–3066.
[12] S.H. Hong, A. Chlenov, M.W. Day, R.H. Grubbs, Angew. Chem. Int. Ed. 46 (2007) 5148–5151.
[13] K.-i. Otake, Y. Cui, C.T. Buru, Z. Li, J.T. Hupp, O.K. Farha, J. Am. Chem. Soc. 140 (2018) 8652–8656.
[14] T. Drake, P. Ji, W. Lin, Acc. Chem. Res. 51 (2018) 2129–2138.
[15] J. Lee, O.K. Farha, J. Roberts, K.A. Scheidt, S.T. Nguyen, J.T. Hupp, Chem. Soc. Rev. 38 (2009) 1450–1459.
[16] H. Furukawa, K.E. Cordova, M. O'Keeffe, O.M. Yaghi,Science 341 (2013), 1230444.
[17] M. O'Keeffe, O.M. Yaghi, Chem. Rev. 112 (2012) 675–702.
[18] J.-S. Qin, S. Yuan, C. Lollar, J. Pang, A. Alsalme, H.-C. Zhou, Chem. Commun. 54 (2018) 4231–4249.
[19] S. Zhao, Y. Wang, J. Dong, C.-T. He, H. Yin, P. An, et al., Nat. Energy 1 (2016) 16184.
[20] L. Jiao, Y. Wang, H.-L. Jiang, Q. Xu,Adv. Mater. 30 (2018), 1703663.
[21] M. Eddaoudi, J. Kim, N. Rosi, D. Vodak, J. Wachter, M. Keeffe, et al., Science 295 (2002) 469–472.
[22] B. Chen, C. Liang, J. Yang, D.S. Contreras, Y.L. Clancy, E.B. Lobkovsky, et al., Angew. Chem. Int. Ed. 45 (2006) 1390–1393.
[23] N.L. Rosi, J. Eckert, M. Eddaoudi, D.T. Vodak, J. Kim, M. Keeffe, et al., Science 300 (2003) 1127–1129.
[24] J. Della Rocca, D. Liu, W. Lin, Acc. Chem. Res. 44 (2011) 957–968.
[25] G. Li, S. Zhao, Y. Zhang, Z. Tang,Adv. Mater. 30 (2018), 1800702.
[26] M. Zhao, K. Yuan, Y. Wang, G. Li, J. Guo, L. Gu, et al., Nature 539 (2016) 76–80.
[27] M. Zhao, K. Deng, L. He, Y. Liu, G. Li, H. Zhao, et al., J. Am. Chem. Soc. 136 (2014) 1738–1741.
[28] W. Zhang, Y. Liu, G. Lu, Y. Wang, S. Li, C. Cui, et al., Adv. Mater. 27 (2015) 2923–2929.
[29] P. Ji, K. Manna, Z. Lin, X. Feng, A. Urban, Y. Song, et al., J. Am. Chem. Soc. 139 (2017) 7004–7011.
[30] S. Yuan, J.-S. Qin, J. Li, L. Huang, L. Feng, Y. Fang, et al., Nat. Commun. 9 (2018) 808.
[31] Y. Peng, H. Huang, Y. Zhang, C. Kang, S. Chen, L. Song, et al., Nat. Commun. 9 (2018) 187.
[32] T. Islamoglu, S. Goswami, Z. Li, A.J. Howarth, O.K. Farha, J.T. Hupp, Acc. Chem. Res. 50 (2017) 805–813.
[33] Z. Liang, C. Qu, D. Xia, R. Zou, Q. Xu, Angew. Chem. Int. Ed. 57 (2018) 9604–9633.
[34] S.M.J. Rogge, A. Bavykina, J. Hajek, H. Garcia, A.I. Olivos-Suarez, A. Sepúlveda-Escribano, et al., Chem. Soc. Rev. 46 (2017) 3134–3184.
[35] A.W. Stubbs, L. Braglia, E. Borfecchia, R.J. Meyer, Y. Román-Leshkov, C. Lamberti, et al., ACS Catal. 8 (2018) 596–601.
[36] P. Ji, K. Manna, Z. Lin, A. Urban, F.X. Greene, G. Lan, et al., J. Am. Chem. Soc. 138 (2016) 12234–12242.
[37] M. Kim, S.M. Cohen, CrystEngComm 14 (2012) 4096–4104.
[38] X. Zhang, Z. Huang, M. Ferrandon, D. Yang, L. Robison, P. Li, et al., Nat. Catal. 1 (2018) 356–362.
[39] S. Ahn, S.L. Nauert, C.T. Buru, M. Rimoldi, H. Choi, N.M. Schweitzer, et al., J. Am. Chem. Soc. 140 (2018) 8535–8543.
[40] P.L. Llewellyn, S. Bourrelly, C. Serre, A. Vimont, M. Daturi, L. Hamon, et al., Langmuir 24 (2008) 7245–7250.
[41] P. Ji, Y. Song, T. Drake, S.S. Veroneau, Z. Lin, X. Pan, et al., J. Am. Chem. Soc. 140 (2018) 433–440.
[42] L. Jiao, H.-L. Jiang, Chem (2019), http://dx.doi.org/10.1016/j.chempr.2018.12.011, in press.
[43] M. Tejeda-Serrano, M. Mon, B. Ross, F. Gonell, J. Ferrando-Soria, A. Corma, et al., J. Am. Chem. Soc. 140 (2018) 8827–8832.
[44] V. Guillerm, F. Ragon, M. Dan-Hardi, T. Devic, M. Vishnuvarthan, B. Campo, et al., Angew. Chem. Int. Ed. 51 (2012) 9267–9271.
[45] J.H. Cavka, S. Jakobsen, U. Olsbye, N. Guillou, C. Lamberti, S. Bordiga, et al., J. Am. Chem. Soc. 130 (2008) 13850–13851.
[46] H. Furukawa, F. Gándara, Y.-B. Zhang, J. Jiang, W.L. Queen, M.R. Hudson, et al., J. Am. Chem. Soc. 136 (2014) 4369–4381.
[47] X. Zhang, X. Zhang, J.A. Johnson, Y.-S. Chen, J. Zhang, J. Am. Chem. Soc. 138 (2016) 8380–8383.
[48] J.E. Mondloch, W. Bury, D. Fairen-Jimenez, S. Kwon, E.J. DeMarco, M.H. Weston, et al., J. Am. Chem. Soc. 135 (2013) 10294–10297.
[49] P. Deria, W. Bury, J.T. Hupp, O.K. Farha, Chem. Commun. 50 (2014) 1965–1968.
[50] C.K. Brozek, M. Dincă, Chem. Soc. Rev. 43 (2014) 5456–5467.
[51] X. Zhang, L. Chang, Z. Yang, Y. Shi, C. Long, J. Han, et al., Nano Res. 12 (2019) 437–440.
[52] I.S. Kim, J. Borycz, A.E. Platero-Prats, S. Tussupbayev, T.C. Wang, O.K. Farha, et al., Chem. Mater. 27 (2015) 4772–4778.
[53] S.T. Madrahimov, J.R. Gallagher, G. Zhang, Z. Meinhart, S.J. Garibay, M. Delferro, et al., ACS Catal. 5 (2015) 6713–6718.
[54] G. Férey, C. Mellot-Draznieks, C. Serre, F. Millange, J. Dutour, S. Surblé, et al., Science 309 (2005) 2040–2042.
[55] H.G.T. Nguyen, M.H. Weston, O.K. Farha, J.T. Hupp, S.T. Nguyen, CrystEngComm 14 (2012) 4115–4118.
[56] Z. Niu, W.D.C. Bhagya Gunatilleke, Q. Sun, P.C. Lan, J. Perman, J.-G. Ma, et al., Chem 4 (2018) 2483–2485.
[57] F. Hoffmann, M. Fröba, J. Getzschmann, W. Böhlmann, S. Kaskel, Microporous Mesoporous Mater. 122 (2009) 93–98.
[58] M. Dan-Hardi, C. Serre, T. Frot, L. Rozes, G. Maurin, C. Sanchez, et al., J. Am. Chem. Soc. 131 (2009) 10857–10859.
[59] Z. Li, A.W. Peters, V. Bernales, M.A. Ortuño, N.M. Schweitzer, M.R. DeStefano, et al., ACS Cent. Sci. 3 (2017) 31–38.
[60] T.A. Goetjen, X. Zhang, J. Liu, J.T. Hupp, O.K. Farha, ACS Sustain. Chem. Eng. 7 (2019) 2553–2557.
[61] R.C. Klet, S. Tussupbayev, J. Borycz, J.R. Gallagher, M.M. Stalzer, J.T. Miller, et al., J. Am. Chem. Soc. 137 (2015) 15680–15683.
[62] H. Noh, Y. Cui, A.W. Peters, D.R. Pahls, M.A. Ortuño, N.A. Vermeulen, et al., J. Am. Chem. Soc. 138 (2016) 14720–14726.
[63] A.M. Abdel-Mageed, B. Rungtaweevoranit, M. Parlinska-Wojtan, X. Pei, O.M. Yaghi, R.J. Behm, J. Am. Chem. Soc. (2019), http://dx.doi.org/10.1021/jacs.8b11386, in press.
[64] H.G.T. Nguyen, N.M. Schweitzer, C.-Y. Chang, T.L. Drake, M.C. So, P.C. Stair, et al., ACS Catal. 4 (2014) 2496–2500.
[65] D. Yang, S.O. Odoh, J. Borycz, T.C. Wang, O.K. Farha, J.T. Hupp, et al., ACS Catal. 6 (2016) 235–247.
[66] A.B. Thompson, D.R. Pahls, V. Bernales, L.C. Gallington, C.D. Malonzo, T. Webber, et al., Chem. Mater. 28 (2016) 6753–6762.
[67] S.P. Desai, J. Ye, J. Zheng, M.S. Ferrandon, T.E. Webber, A.E. Platero-Prats, et al., J. Am. Chem. Soc. 140 (2018) 15309–15318.
[68] Y. Song, Z. Li, P. Ji, M. Kaufmann, X. Feng, J.S. Chen, et al., ACS Catal. 9 (2019) 1578–1583.
[69] C.K. Brozek, J.T. Miller, S.A. Stoian, M. Dincă, J. Am. Chem. Soc. 137 (2015) 7495–7501.
[70] H. Fei, J.F. Cahill, K.A. Prather, S.M. Cohen, Inorg. Chem. 52 (2013) 4011–4016.
[71] D. Denysenko, T. Werner, M. Grzywa, A. Puls, V. Hagen, G. Eickerling, et al., Chem. Commun. 48 (2012) 1236–1238.
[72] R.J. Comito, K.J. Fritzsching, B.J. Sundell, K. Schmidt-Rohr, M. Dincă, J. Am. Chem. Soc. 138 (2016) 10232–10237.
[73] D. Denysenko, J. Jelic, K. Reuter, D. Volkmer, Chem. Eur. J. 21 (2015) 8188–8199.
[74] R.J.C. Dubey, R.J. Comito, Z. Wu, G. Zhang, A.J. Rieth, C.H. Hendon, et al., J. Am. Chem. Soc. 139 (2017) 12664–12669.
[75] R.J. Comito, Z. Wu, G. Zhang, J.A. Lawrence, M.D. Korzyński, J.A. Kehl, et al., Angew. Chem. Int. Ed. 57 (2018) 8135–8139.
[76] A. Bajpai, P. Chandrasekhar, S. Govardhan, R. Banerjee, J.N. Moorthy, Chem. Eur. J. 21 (2015) 2759–2765.
[77] Z. Li, N.M. Schweitzer, A.B. League, V. Bernales, A.W. Peters, A.B. Getsoian, et al., J. Am. Chem. Soc. 138 (2016) 1977–1982.
[78] A.W. Peters, Z. Li, O.K. Farha, J.T. Hupp, ACS Nano 9 (2015) 8484–8490.
[79] I.S. Kim, Z. Li, J. Zheng, A.E. Platero-Prats, A. Mavrandonakis, S. Pellizzeri, et al., Angew. Chem. Int. Ed. 57 (2018) 909–913.
[80] J. Liu, J. Ye, Z. Li, K.-i. Otake, Y. Liao, A.W. Peters, et al., J. Am. Chem. Soc. 140 (2018) 11174–11178.
[81] D. Yang, M.R. Momeni, H. Demir, D.R. Pahls, M. Rimoldi, T.C. Wang, et al., Faraday Discuss. 201 (2017) 195–206.
[82] S. Ahn, N.E. Thornburg, Z. Li, T.C. Wang, L.C. Gallington, K.W. Chapman, et al., Inorg. Chem. 55 (2016) 11954–11961.
[83] L.C. Gallington, I.S. Kim, W.-G. Liu, A.A. Yakovenko, A.E. Platero-Prats, Z. Li, et al., J. Am. Chem. Soc. 138 (2016) 13513–13516.
[84] O.K. Farha, J.T. Hupp, Acc. Chem. Res. 43 (2010) 1166–1175.
[85] K.K. Tanabe, C.A. Allen, S.M. Cohen, Angew. Chem. Int. Ed. 49 (2010) 9730–9733.
[86] Z. Wang, S.M. Cohen, Chem. Soc. Rev. 38 (2009) 1315–1329.

[87] Y.K. Hwang, D.-Y. Hong, J.-S. Chang, S.H. Jhung, Y.-K. Seo, J. Kim, et al., Adv. Mater. 120 (2008) 4212–4216.
[88] B.J. Burnett, P.M. Barron, C. Hu, W. Choe, J. Am. Chem. Soc. 133 (2011) 9984–9987.
[89] O. Karagiaridi, W. Bury, J.E. Mondloch, J.T. Hupp, O.K. Farha, Angew. Chem. Int. Ed. 53 (2014) 4530–4540.
[90] Y. Zhang, J. Guo, L. Shi, Y. Zhu, K. Hou, Y. Zheng, et al.,Sci. Adv. 3 (2017), e1701162.
[91] A.M. Shultz, O.K. Farha, D. Adhikari, A.A. Sarjeant, J.T. Hupp, S.T. Nguyen, Inorg. Chem. 50 (2011) 3174–3176.
[92] S. Wu, L. Chen, B. Yin, Y. Li, Chem. Commun. 51 (2015) 9884–9887.
[93] T. Zhang, K. Manna, W. Lin, J. Am. Chem. Soc. 138 (2016) 3241–3249.
[94] M. Liu, Y.-F. Mu, S. Yao, S. Guo, X.-W. Guo, Z.-M. Zhang, et al., Appl. Catal. B 245 (2019) 496–501.
[95] T. Toyao, K. Miyahara, M. Fujiwaki, T.-H. Kim, S. Dohshi, Y. Horiuchi, et al., J. Phys. Chem. C 119 (2015) 8131–8137.
[96] R. Huang, Y. Peng, C. Wang, Z. Shi, W. Lin, Eur. J. Inorg. Chem. 2016 (2016) 4358–4362.
[97] B. An, L. Zeng, M. Jia, Z. Li, Z. Lin, Y. Song, et al., J. Am. Chem. Soc. 139 (2017) 17747–17750.
[98] S. Yang, B. Pattengale, S. Lee, J. Huang, ACS Energy Lett. 3 (2018) 532–539.
[99] D. Dong, Z. Li, D. Liu, N. Yu, H. Zhao, H. Chen, et al., New J. Chem. 42 (2018) 9317–9323.
[100] L. Cao, Z. Lin, F. Peng, W. Wang, R. Huang, C. Wang, et al., Angew. Chem. Int. Ed. 55 (2016) 4962–4966.
[101] X. Fang, Q. Shang, Y. Wang, L. Jiao, T. Yao, Y. Li, et al.,Adv. Mater. 30 (2018), 1705112.
[102] F. Leng, H. Liu, M. Ding, Q.-P. Lin, H.-L. Jiang, ACS Catal. 8 (2018) 4583–4590.
[103] T. He, S. Chen, B. Ni, Y. Gong, Z. Wu, L. Song, et al., Angew. Chem. Int. Ed. 57 (2018) 3493–3498.
[104] T. Sawano, Z. Lin, D. Boures, B. An, C. Wang, W. Lin, J. Am. Chem. Soc. 138 (2016) 9783–9786.
[105] S.G. Dunning, G. Nandra, A.D. Conn, W. Chai, R.E. Sikma, J.S. Lee, et al., Angew. Chem. Int. Ed. 57 (2018) 9295–9299.
[106] A. Grigoropoulos, A.I. McKay, A.P. Katsoulidis, R.P. Davies, A. Haynes, L. Brammer, et al., Angew. Chem. Int. Ed. 57 (2018) 4532–4537.
[107] K. Manna, T. Zhang, M. Carboni, C.W. Abney, W. Lin, J. Am. Chem. Soc. 136 (2014) 13182–13185.
[108] M.A. Gotthardt, R. Schoch, T.S. Brunner, M. Bauer, W. Kleist, ChemPlusChem 80 (2015) 188–195.
[109] N.C. Thacker, Z. Lin, T. Zhang, J.C. Gilhula, C.W. Abney, W. Lin, J. Am. Chem. Soc. 138 (2016) 3501–3509.
[110] S. Roy, A. Bhunia, N. Schuth, M. Haumann, S. Ott, Sustain. Energy Fuels 2 (2018) 1148–1152.
[111] Z. Huang, D. Liu, J. Camacho-Bunquin, G. Zhang, D. Yang, J.M. López-Encarnación, et al., Organometallics 36 (2017) 3921–3930.
[112] H. Fei, J. Shin, Y.S. Meng, M. Adelhardt, J. Sutter, K. Meyer, et al., J. Am. Chem. Soc. 136 (2014) 4965–4973.
[113] H. Fei, S.M. Cohen, J. Am. Chem. Soc. 137 (2015) 2191–2194.
[114] M.B. Chambers, X. Wang, N. Elgrishi, C.H. Hendon, A. Walsh, J. Bonnefoy, et al., ChemSusChem 8 (2015) 603–608.
[115] K.K. Tanabe, S.M. Cohen, Angew. Chem. Int. Ed. 121 (2009) 7560–7563.
[116] S.M. Cohen, Chem. Rev. 112 (2012) 970–1000.
[117] R.W. Larsen, L. Wojtas, J. Perman, R.L. Musselman, M.J. Zaworotko, C.M. Vetromile, J. Am. Chem. Soc. 133 (2011) 10356–10359.
[118] B. Nepal, S. Das, Angew. Chem. Int. Ed. 125 (2013) 7365–7368.
[119] R.E. Hansen, S. Das, Energy Environ. Sci. 7 (2014) 317–322.
[120] Z. Li, T.M. Rayder, L. Luo, J.A. Byers, C.-K. Tsung, J. Am. Chem. Soc. 140 (2018) 8082–8085.
[121] M. Mihaylov, E. Ivanova, F. Thibault-Starzyk, M. Daturi, L. Dimitrov, K. Hadjiivanov, J. Phys. Chem. B 110 (2006) 10383–10389.
[122] J. Liang, Z. Liang, R. Zou, Y. Zhao,Adv. Mater. 29 (2017), 1701139.
[123] M. Ranocchiari, C. Lothschütz, D. Grolimund, A. van Bokhoven Jeroen, Proc. Math. Phys. Eng. Sci. 468 (2012) 1985–1999.
[124] Z. Lounis, A. Riahi, F. Djafri, J. Muzart, Appl. Catal. A Gen. 309 (2006) 270–272.
[125] D. Zhu, C. Guo, J. Liu, L. Wang, Y. Du, S.-Z. Qiao, Chem. Commun. 53 (2017) 10906–10909.
[126] Y. Pei, Z. Qi, X. Li, R.V. Maligal-Ganesh, T.W. Goh, C. Xiao, et al., J. Mater. Chem. A 5 (2017) 6186–6192.
[127] S. Yuan, P. Zhang, L. Zhang, A.T. Garcia-Esparza, D. Sokaras, J.-S. Qin, et al., J. Am. Chem. Soc. 140 (2018) 10814–10819.
[128] X. Li, T.W. Goh, L. Li, C. Xiao, Z. Guo, X.C. Zeng, et al., ACS Catal. 6 (2016) 3461–3468.
[129] Z. Guo, T. Kobayashi, L.-L. Wang, T.W. Goh, C. Xiao, M.A. Caporini, et al., Chem. Eur. J. 20 (2014) 16308–16313.
[130] G. Lan, Z. Li, S.S. Veroneau, Y.-Y. Zhu, Z. Xu, C. Wang, et al., J. Am. Chem. Soc. 140 (2018) 12369–12373.
[131] X. Li, Z. Guo, C. Xiao, T.W. Goh, D. Tesfagaber, W. Huang, ACS Catal. 4 (2014) 3490–3497.
[132] R. Limvorapitux, L.-Y. Chou, A.P. Young, C.-K. Tsung, S.T. Nguyen, ACS Catal. 7 (2017) 6691–6698.
[133] X. Li, B. Zhang, L. Tang, T.W. Goh, S. Qi, A. Volkov, et al., Angew. Chem. Int. Ed. 56 (2017) 16371–16375.
[134] Y.-Y. Zhu, G. Lan, Y. Fan, S.S. Veroneau, Y. Song, D. Micheroni, et al., Angew. Chem. Int. Ed. 130 (2018) 14286–14290.
[135] P.V. Dau, S.M. Cohen, Chem. Commun. 49 (2013) 6128–6130.
[136] P.V. Dau, S.M. Cohen, Inorg. Chem. 54 (2015) 3134–3138.
[137] X. Li, R. Van Zeeland, R.V. Maligal-Ganesh, Y. Pei, G. Power, L. Stanley, et al., ACS Catal. 6 (2016) 6324–6328.
[138] P.J. Larson, J.L. Cheney, A.D. French, D.M. Klein, B.J. Wylie, A.F. Cozzolino, Inorg. Chem. 57 (2018) 6825–6832.
[139] H. Noh, C.-W. Kung, K.-i. Otake, A.W. Peters, Z. Li, Y. Liao, et al., ACS Catal. 8 (2018) 9848–9858.
[140] A.E. Platero-Prats, A.B. League, V. Bernales, J. Ye, L.C. Gallington, A. Vjunov, et al., J. Am. Chem. Soc. 139 (2017) 10410–10418.
[141] T. Sawano, P. Ji, A.R. McIsaac, Z. Lin, C.W. Abney, W. Lin, Chem. Sci. 6 (2015) 7163–7168.
[142] J.A. Johnson, B.M. Petersen, A. Kormos, E. Echeverría, Y.-S. Chen, J. Zhang, J. Am. Chem. Soc. 138 (2016) 10293–10298.

Wenshi Zhao received his BS degree of chemistry from Lanzhou University in 2016 and joined Prof. Zhiyong Tang's group in National Center for Nanoscience and Technology as a PhD candidate. His research interest focuses on design and synthesis of metal-organic frameworks for catalysis.

Professor Guodong Li received his BS degree from University of Jinan in 2004, MS degree from Ocean University of China in 2007, and PhD degree from Beijing University of Chemical Technology in 2011. Then, he joined National Center for Nanoscience and Technology. He was also a visiting scholar in Stanford University from 2016 to 2017. His research interestsare focused on design and fabrication of inorganic nanocomposites with well-defined structures as well as their application in catalysis and energy.

Professor Zhiyong Tang obtained his PhD degree from Chinese Academy of Sciences in 2000 under the direction of Professor Erkang Wang. After finishing his postdoctoral training at both Swiss Federal Institute of Technology Zurich and University of Michigan, he came back to China and took a professor position at National Center for Nanoscience and Technology at the end of 2006. His main research interests are focused on preparation, assembly, and application of functional nanomaterials.